STAR-RIS Assisted MISO-NOMA Networks: A Simultaneous Signal Enhancement and Interference Mitigation Design

Jie Li, Zhengyu Song, Tianwei Hou, *Member, IEEE,* Chongwen Huang, *Member, IEEE,* Anna Li, *Member, IEEE,* Gui Zhou, *Member, IEEE,* Yuanwei Liu, *Fellow, IEEE*

***Abstract*—Simultaneous transmitting and reflecting (STAR) reconfigurable intelligent surface (RIS) technique has recently received considerable attention due to its omni-directional radiation capability. In this paper, motivated by the interference-mitigation-based (IMB) and signal-enhancement-based (SEB) designs, we introduce an innovative STAR-RIS assisted simultaneous-signal-enhancement-and-interference-mitigation (SSEIM) design in non-orthogonal multiple access (NOMA) multiple-input single-output cellular communication networks. Our objective is to maximize the system spectral efficiency (SE) by jointly optimizing the reflection and transmission phase shifts at the STAR-RIS, the precoding matrix of BSs, and the power allocation factors of NOMA users. We propose a low-complexity simultaneous enhancement and mitigation algorithm. Furthermore, by exploiting the manifold optimization technique, we introduce the Riemannian conjugate gradient algorithm to solve the non-convex subproblems with unit modulus constraint. Our analysis reveals that the proposed SSEIM design exceeds the traditional RIS-aided SEB and IMB designs.**

***Index Terms*—Active beamforming, STAR-RIS, NOMA, SSEIM, manifold optimization.**

I. Introduction

Reconfigurable intelligent surfaces (RISs) are emerging as a pivotal technology in the advancement of 6G networks. By manipulating electromagnetic waves via a controllable array of passive elements, RISs offer transformative benefits, such as easy deployment, environment-friendly, low cost, enhanced coverage, high energy efficiency (EE) and superior spectral efficiency (SE) [1]–[4]. In addition, RISs have extensive application prospects for vehicular, robotic, visible light communications, and near-field communications [5]–[7]. Despite the promising capabilities of RISs, traditional designs have been limited to signal reflection, thereby restricting the service coverage to 180 degrees. The advent of simultaneous transmitting and reflecting RIS (STAR-RIS) technology addresses the limitation, enabling full 360-degree coverage and opening new avenues for wireless communication enhancements [8]–[10]. Specifically, the signal model based on dual-sided STAR-RIS, as presented in [11], improves signal transmission and coverage by reflecting signals in two opposite directions simultaneously. The advanced dual-sided STAR-RIS significantly extends coverage and addresses modern communication challenges effectively [12]–[14].

Recently, the research on RIS/STAR-RIS enhanced networks is mainly divided into two categories: interference-mitigation-based (IMB) [15], [16] and signal-enhancement-based (SEB) designs [17], [18]. In [17], an RIS-assisted multiple-input multiple-output (MIMO) network was proposed, where the desired signal can be adjusted by managing the reflection coefficients of RIS elements. In the millimeter wave assisted mobile scenario, STAR-RIS can enhance the received signal of both roadside units and in-vehicle users [18]. Unfortunately, the interferences will be increased with the support of SEB design, which significantly limits the network performance in the high signal-to-noise-ratio (SNR) scenarios. In contrast, an uplink heterogeneous network joint integrating non-orthogonal multiple access (NOMA) and AirFL framework was proposed, where STAR-RIS is utilized to eliminate co-channel interferences [19]. With the rapid expansion of base stations (BSs), an RIS-NOMA-enhanced IMB design was proposed in [20], which mitigates both inter-cluster and inter-cell interferences. However, the IMB design fails to enhance the desired signal, which constrains the communication performance in low-SNR scenarios. To improve the performance in both high-SNR and low-SNR regimes, a novel concept of simultaneous-signal-enhancement-and-cancellation-based (SSECB) was proposed in [21], which is capable of enhancing and mitigating the desired signals and the interference signals simultaneously.

This work was supported in part by the Fundamental Research Funds for the Central Universities under Grant 2024JBMC014 and 2023JBZY012, in part by the National Natural Science Foundation for Young Scientists of China under Grant 62201028, in part by Young Elite Scientists Sponsorship Program by CAST under Grant 2022QNRC001, in part by the Beijing Natural Science Foundation L232041, and in part by the Marie Skłodowska-Curie Fellowship under Grant 101106428 and 101154499. An earlier version of this paper was presented in part at the IEEE Global Communication Conference, Cape Town, South Africa, 8-12 Dec, 2024. (Corresponding author: Tianwei Hou.)

J. Li is with the China Mobile Research and Development Center for Network Planning and Optimization, China Mobile Group Design Institute Company Ltd., Beijing 100080, China (email: 21120077@bjtu.edu.cn).

Z. Song is with the School of Electronic and Information Engineering, Beijing Jiaotong University, Beijing 100044, China (email: songzy@bjtu.edu.cn).

T. Hou is with the School of Electronic and Information Engineering, Beijing Jiaotong University, Beijing 100044, China, and also with School of Electronic Engineering and Computer Science, Queen Mary University of London, London E1 4NS, U.K. (email: twhou@bjtu.edu.cn).

C. Huang is with College of Information Science and Electronic Engineering, Zhejiang University, Hangzhou 310027, China. (E-mail: chongwenhuang@zju.edu.cn).

A. Li is with the School of Computing and Communications, Lancaster University, Lancaster, U.K., and is also with Katholieke Universiteit Leuven (KU Leuven), Leuven, Belgium. (e-mail: a.li16@lancaster.ac.uk).

G. Zhou is with Institute for Digital Communications, Friedrich-Alexander Universität Erlangen-Nürnberg (FAU), 91054 Erlangen, Germany. (e-mail: gui.zhou@fau.de).

Y. Liu is with the Department of Electrical and Electronic Engineering, The University of Hong Kong, Hong Kong (e-mail: yuanwei@hku.hk).

Leveraging STAR-RIS arrays, the SSECB design of the NOMA coordinated multi-point transmission networks can be accomplished. However, only the simplest single-input single-output scenario is considered in [21]. In actual multi-antenna scenarios, the beamforming at the BSs and the correlation of channels need to be considered [22]–[24]. In a double-RIS-aided MISO network, the spatial correlation of RISs can improve the achievable rate, whereas there is a negative impact on the transmit correlation at BSs [22]. Moreover, STAR-RIS inherently has a complex parameter space. Numerous parameters are mixed up with each other, which makes it difficult to solve optimization problems. The currently available algorithms are of high complexity, which demand a large amount of computing and time resources [25], [26].

The integration of NOMA and STAR-RISs can provide synergistic advantages, such as supporting massive connectivity, enhancing SE, and facilitating flexible resource allocation by intelligently controlling the channel state information (CSI) of users [27]–[30]. However, traditional RIS can only reflect signals, resulting in similar channel conditions for users in the reflected space, which limits the full advantages of NOMA. Therefore, the application prospect of STAR-RIS-NOMA networks has been explored [31]–[35]. In [31], a STAR-RIS assisted NOMA downlink (DL) architecture was proposed, where the effective channel capacity was improved. Then, the data rate of STAR-RIS-NOMA assisted communication system in the case of statistical CSI is analyzed in [32]. The joint optimization of passive beamforming at STAR-RIS, the decoding order and the active beamforming at BS was proposed in [35], maximizing the achievable sum data rate.

A. Motivations and Contributions

Existing research predominantly focuses on RIS-assisted SEB design or RIS-assisted IMB design [16]–[19]. In practical applications, the signal enhancement design will also enhance the interferences, while the interference mitigation design will not enhance any desired signals. Therefore, it is urgent to find a scheme for enhancing and mitigating the desired signals and the interference signals simultaneously, which poses two critical challenges: i) Traditional RIS cannot deliver full-space communication services to massive users, integrating STAR-RIS with NOMA techniques into cellular networks is essential. ii) Compared to traditional RIS, STAR-RIS necessitates optimization within a more complex parameter space, demanding enhanced computational capabilities and algorithmic support. Moreover, An increase in the number of parameters may compromise system stability and reliability, making existing research approaches complex and challenging to implement in practice. To tackle these issues while offering valuable engineering insights, we present an innovative low-complexity simultaneous-signal-enhancement-and-interference-mitigation (SSEIM) design tailored for dual-sided STAR-RISs assisted MISO-NOMA cellular networks. The primary contributions are concluded as follows:

- An innovative SSEIM design for a dual-sided STAR-RISs assisted multiuser MISO-NOMA downlink cellular network is proposed. With STAR-RIS deployed at the junction of two cells, the SSEIM design can enhance and mitigate the desired signals and the interference signals simultaneously. The reflected signal is used to enhance the desired signals, while the transmitted signal is used to mitigate interference signals, which are defined as SEB-sector and IMB-sector, respectively.
- We develop an optimization problem aimed at maximizing SE and present a systematic approach by partitioning it into three sub-problems. First, for the SEB-sector, we utilize the maximum ratio transmission (MRT) precoding matrix to optimize the reflection phase shifts of STAR-RIS and the active beamformer at BSs jointly. Next, for the IMB-sector, we optimize the transmission phase shifts of STAR-RIS to mitigate both inter-cell and intra-cell interferences. Finally, we optimize the NOMA power allocation factors based on the target data rates.
- We propose a low-complexity simultaneous enhancement and mitigation (LSEM) algorithm. By exploiting the complex circle manifold optimization technique, the unit modulus constraints can be effectively addressed by the Riemannian conjugate gradient (RCG) algorithm. Additionally, we consider the effects of spatial correlation and determine the minimum required number of STAR-RIS elements for the IMB-sector.
- Our numerical results demonstrate that: 1) Compared to the RIS-aided SEB and IMB designs, the EE and SE of our proposed STAR-RIS assisted SSEIM design are significantly improved; 2) Compared with the zero forcing (ZF) precoding and identity precoding matrices, the proposed SSEIM design has superior performance in the case of MRT precoding matrix; 3) There is an optimal range of the reflection power coefficient, which indicates that a tradeoff exists between SEB-sector and IMB-sector.

B. Organization and Notations

In Section II, we present a dual-sided STAR-RIS aided multiuser MISO-NOMA DL cellular communication network model, and the corresponding optimization problem is formulated. We propose a LSEM algorithm to solve the optimization problem. Specifically, the RCG algorithm is utilized to solve both SEB-sector and IMB-sector subproblems in Section III and Section IV. Numerical results are given in Section V to demonstrate the effectiveness of the proposed STAR-RIS assisted SSEIM design. Finally, Section VI provides the conclusion and outlines potential future applications.

Notations: $\mathbf{H}^*$, $\mathbf{H}^H$ and $\mathbf{H}^T$ denote the conjugate, conjugate transpose and transpose of the matrix $\mathbf{H}$, respectively. $\circ$ and $\otimes$ represent the Hadamard product and the Kronecker product, respectively. $\mathrm{diag}[\cdot]$ symbolizes a diagonal matrix. $|\bullet|$ and $\|\bullet\|_2$ denote the absolute value and the Frobenius norm, respectively. $\mathcal{C}^L$ is the space of $L \times 1$ complex vector.

II. System Model and Problem Formulation

A. System Model

We consider a dual-sided STAR-RIS assisted multiuser MISO-NOMA downlink cellular communication network, as depicted in Fig. 1. The network comprises a STAR-RIS, two

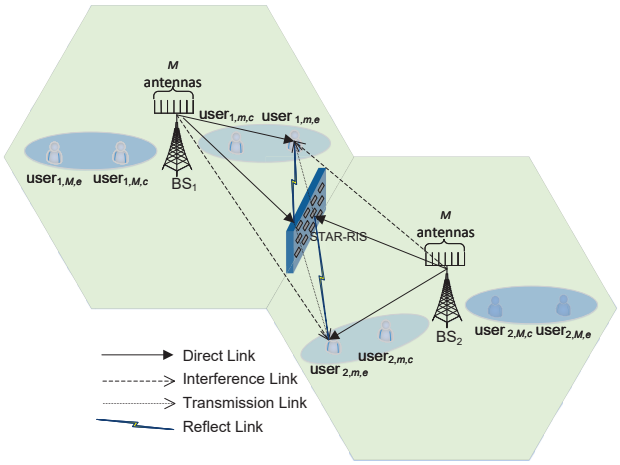

Fig. 1: STAR-RIS assisted cellular MISO-NOMA downlink network.

cells, two base stations (BSs), and M clusters in each cell. The BS situated at the center of the cell is equipped with M transmitting antennas (TAs) that are arranged in a uniform linear array (ULA). Each cluster contains two users, namely the cell-center user (CCU) and cell-edge user (CEU) based on the distance from BS to user. Each user has a single receiving antenna. All users can receive the direct link signals, the signals reflected by STAR-RIS, the signals transmitted by STAR-RIS, and the channel noise[1].

A dual-sided uniform planar array (UPA) STAR-RIS is deployed at the junction of two cells with $L = L_H \times L_V$ passive STAR-RIS elements. Utilizing energy splitting (ES) protocol, the STAR-RIS elements can transmit and reflect signals simultaneously [10]. After the signal from the BS 1 reaches the STAR-RIS, the dual-sided STAR-RIS reflects it to the users in cell 1 and transmit it to the users in cell 2. Based on the insights of [9] and [33], we also consider the ES factor for the transmitted and reflected signals to be uniform across all STAR-RIS elements, while the phase shift of each STAR-RIS element can be adjusted independently. Since the signals from BS do not carry the information of the users in adjacent cells, the signals transmitted by STAR-RIS are all used to mitigate the interferences. In order to implement the proposed SSEIM design, the signals reflected by STAR-RIS are used to amplify the desired signals, thus improving the overall communication quality.

B. Channel Model

In this paper, both line-of-sight (LoS) and non-LoS (NLoS) components are considered in the BS-user links. We model the channels from the BS located in cell $i \in \{1, 2\}$ to the CCU in the m-th cluster of cell i as spatially correlated Rician fading channels

$$\mathbf{w}_{i,i,m,c} = \sqrt{\frac{\mathcal{K}_1}{\mathcal{K}_1+1}}\mathbf{w}_{i,i,m,c}^{\mathrm{LoS}} + \sqrt{\frac{1}{\mathcal{K}_1+1}}\mathbf{w}_{i,i,m,c}^{\mathrm{NLoS}}\mathbf{R}_d^{1/2}, \quad (1)$$

[1]The direct link signal from BS to users within the same cell is inter-cluster interference and the desired signal, whereas the direct link signal from BS to users in the adjacent cell results in inter-cell interference.

where $\mathbf{w}_{i,i,m,c}^{\mathrm{LoS}}$ and $\mathbf{w}_{i,i,m,c}^{\mathrm{NLoS}}$ are the LoS and NLoS components with $(1 \times M)$ elements. $\mathcal{K}$ is the Rician factor, representing the power ratio between LoS and NLoS components. $\mathbf{R}_d$ denotes the BS transmit correlation matrix with $(M \times M)$ elements. By utilizing the exponential model, the ULA spatial correlation matrix is represented as follows [22]–[24]

$$R_d(x,y) = \begin{cases} \left(r_d e^{j'\vartheta}\right)^{y-x}, & \text{if} \quad x \le y, \\ \left(\left(r_d e^{j'\vartheta}\right)^*\right)^{x-y}, & \text{otherwise}, \end{cases} \quad (2)$$

where $R_d(x,y)$ denotes the element in the y-th column and x-th row of matrix $\mathbf{R}_d$. The correlation coefficient is set to $r_d \in [0,1]$, the corresponding vertical or horizontal angle of departure (AoD) is denoted by ϑ, the imaginary unit is represented by $j' = \sqrt{-1}$.

Since many obstacles are located between users and the BS in the adjacent cell, the channel from the BS located in cell i to the CCU in cluster m of cell j $(j \in \{1,2\}, j \neq i)$ is expressed as

$$\mathbf{w}_{i,j,m,c} = \left[\begin{array}{ccc} w_1^{i,j,m,c} & \cdots & w_M^{i,j,m,c} \end{array}\right], \quad (3)$$

where $\mathbf{w}_{i,j,m,c}$ is a $(1 \times M)$ vector, which follows Rayleigh distribution. $f(x) = e^{-x}$ is the probability density function.

The dual-sided STAR-RIS UPA can reflect and transmit signals from the BS in cell 1 and the BS in cell 2. Similar to (1), we define the spatial correlation channel matrix from BS i to STAR-RIS as

$$\mathbf{F}_i = \sqrt{\frac{\mathcal{K}_2}{\mathcal{K}_2+1}}\mathbf{F}_i^{\mathrm{LoS}} + \sqrt{\frac{1}{\mathcal{K}_2+1}}\mathbf{R}_R^{1/2}\mathbf{F}_i^{\mathrm{NLoS}}\mathbf{R}_d^{1/2}, \quad (4)$$

where $\mathbf{F}_i$ is a $(L \times M)$ matrix, which follows the Rician distribution. $\mathbf{F}_i^{\mathrm{LoS}}$ stands for the LoS component, while $\mathbf{F}_i^{\mathrm{NLoS}}$ stands for the NLoS component. $\mathbf{R}_R$ is a $(L \times L)$ receiving correlation matrix of STAR-RIS. It can be approximated exploiting the Kronecker model as

$$\mathbf{R}_R \approx \mathbf{R}_{R,H} \otimes \mathbf{R}_{R,V}, \quad (5)$$

where $\mathbf{R}_{R,V} \in \mathcal{C}^{\sqrt{L}\times\sqrt{L}}$ and $\mathbf{R}_{R,H} \in \mathcal{C}^{\sqrt{L}\times\sqrt{L}}$ are the vertical ULA and horizontal ULA correlation matrices, respectively.

In the proposed networks, the channel from the STAR-RISs to the CCU in cluster m of cell i can be modeled as

$$\mathbf{g}_{i,m,c} = \sqrt{\frac{\mathcal{K}_3}{\mathcal{K}_3+1}}\mathbf{g}_{i,m,c}^{\mathrm{LoS}} + \sqrt{\frac{1}{\mathcal{K}_3+1}}\mathbf{g}_{i,m,c}^{\mathrm{NLoS}}\mathbf{R}_{R,i,m,c}^{1/2}, \quad (6)$$

where $\mathbf{g}_{i,m,c}$ is a $(1 \times L)$ vector, which follows Rician distribution. $\mathbf{g}_{i,m,c}^{\mathrm{LoS}}$ stands for the LoS component, while $\mathbf{g}_{i,m,c}^{\mathrm{NLoS}}$ stands for the NLoS component. $\mathbf{R}_{R,u}$ is the spatial correlation matrix between the users and the STAR-RIS. Similar to (5), it can be represented as the Kronecker product of the vertical and horizontal correlation matrix.

We then pay attention to the impact of the path loss, and the large-scale fading from BS i to CCU in cluster m of cell j $(i \neq j)$ is represented as

$$\varepsilon_{i,j,m,c} = d_{i,j,m,c}^{-\alpha_1}, \quad (7)$$

where α_1 is the path loss exponent for the BS-user link in different cell, $d_{i,j,m,c}$ is the distance between BS i and CCU

of cluster m located in the adjacent cell.

With the distance $d_{i,i,m,c}$ between BS i and CCU of cluster m within the same cell, the path loss exponent α_2, the large-scale fading of BS-user link can be calculated by

$$\varepsilon_{i,i,m,c} = d_{i,i,m,c}^{-\alpha_2}. \tag{8}$$

The STAR-RIS is deployed at the border of two cells, we consider the large-scale fading of BS-RIS-user links as LoS links. The large-scale fading from BS i to the CCU in cluster m of cell j through STAR-RIS is represented to be

$$\varepsilon_{i,\mathrm{R},j,m,c} = d_{i,\mathrm{R}}^{-\alpha_3} d_{\mathrm{R},j,m,c}^{-\alpha_4}, \tag{9}$$

where the distance from the STAR-RIS to CCU in cluster m of cell j and from the BS i to the STAR-RIS are given by $d_{\mathrm{R},j,m,c}$ and $d_{i,\mathrm{R}}$, respectively. The path loss exponents of the RIS-user and BS-RIS links can be defined as α_3 and α_4, respectively.

C. Signal Model

The information bearing vector transmitted by BS i can be denoted by

$$\mathbf{s}_i = \begin{bmatrix} \alpha_c s_{i,1,c} + \alpha_e s_{i,1,e} \\ \vdots \\ \alpha_c s_{i,m,c} + \alpha_e s_{i,m,e} \\ \vdots \\ \alpha_c s_{i,M,c} + \alpha_e s_{i,M,e} \end{bmatrix}, \tag{10}$$

where $\mathbf{s}_i$ contains M elements. α_c and α_e are the power allocation factors of CCU and CEU with $\alpha_c^2 + \alpha_e^2 = 1$, respectively. The transmitted symbol for CCU and CEU of the m-th cluster in BS i is denoted by $s_{i,m,c}$ and $s_{i,m,e}$, respectively.

Due to the symmetry of dual-sided STAR-RIS [11], the reflection coefficients are identical for both leftward and rightward reflections, and the transmission coefficients from the left are equivalent to those from the right. The reflection and transmission coefficients are independent, which are defined as follows:

$$\begin{aligned} \mathbf{\Phi}_R &\triangleq \mathrm{diag}\left[\beta_{R,1}\phi_{R,1}, \cdots, \beta_{R,L}\phi_{R,L}\right], \\ \mathbf{\Phi}_T &\triangleq \mathrm{diag}\left[\beta_{T,1}\phi_{T,1}, \cdots, \beta_{T,L}\phi_{T,L}\right], \end{aligned} \tag{11}$$

where $\beta_{R,l} \in (0,1]$ and $\beta_{T,l} \in (0,1]$ are the reflected and transmitted amplitude coefficients of the l-th STAR-RIS element, respectively. $\phi_{R,l} = \exp(j'\theta_{R,l})$ and $\phi_{T,l} = \exp(j'\theta_{T,l})$ are the corresponding phase shifts, satisfying $\theta_{R,l} \in [0, 2\pi), \theta_{T,l} \in [0, 2\pi)$.

Independent adjustment of the transmission and reflection phase shifts are possible for each passive STAR-RIS element [10], [33], [36], while due to energy conservation law, the total power of reflection and transmission coefficients is constrained to

$$\beta_{R,l}^2 + \beta_{T,l}^2 \leq 1, \forall l = 1, \cdots, L, \tag{12}$$

where we set $\beta_{R,l}^2 + \beta_{T,l}^2 = 1$ for simplicity.

Similar to [11], the amplitude coefficients are assumed to be identical, i.e., $\beta_{R,l} = \beta_R, \beta_{T,l} = \beta_T, \forall l = 1, \cdots, L$. Then, the STAR-RIS coefficient matrix is further simplified to

$$\begin{aligned} \mathbf{\Phi}_R &= \beta_R \mathrm{diag}\left[e^{j'\theta_{R,1}}, \cdots, e^{j'\theta_{R,L}}\right], \\ \mathbf{\Phi}_T &= \beta_T \mathrm{diag}\left[e^{j'\theta_{T,1}}, \cdots, e^{j'\theta_{T,L}}\right]. \end{aligned} \tag{13}$$

We define the transmit power and the precoding matrix of the i-th BS as p_i and $\mathbf{P}_i$, respectively. Hence, the received signal of users in cluster m of cell 1 is represented as

$$\begin{aligned} y_{1,m,k} = &\sqrt{\varepsilon_{1,1,m,k}}\mathbf{w}_{1,1,m,k}\mathbf{P}_1\sqrt{p_1}\mathbf{s}_1 \\ &+ \sqrt{\varepsilon_{1,\mathrm{R},1,m,k}}\mathbf{g}_{1,m,k}\mathbf{\Phi}_R\mathbf{F}_1\mathbf{P}_1\sqrt{p_1}\mathbf{s}_1 \\ &+ \sqrt{\varepsilon_{2,1,m,k}}\mathbf{w}_{2,1,m,k}\mathbf{P}_2\sqrt{p_2}\mathbf{s}_2 \\ &+ \sqrt{\varepsilon_{2,\mathrm{R},1,m,k}}\mathbf{g}_{1,m,k}\mathbf{\Phi}_T\mathbf{F}_2\mathbf{P}_2\sqrt{p_2}\mathbf{s}_2 + N_0^{1,m,k}, \end{aligned} \tag{14}$$

where $k \in \{c, e\}$, N_0 is the additive white Gaussian noise (AWGN), which has variance σ^2 and mean 0.

D. Analysis of Desired Signal and Interference

Based on the dual-sided STAR-RIS assisted SSEIM design, we enhance the desired signals by superimposing them with the STAR-RIS-reflected signals. Consequently, we can represent the effective channel gains of the CCU and CEU in cluster m of cell i as

$$\begin{aligned} &|h|_{i,m,c}^2 = \\ &\left|\left(\sqrt{\varepsilon_{i,i,m,c}}\mathbf{w}_{i,i,m,c} + \sqrt{\varepsilon_{i,\mathrm{R},i,m,c}}\mathbf{g}_{i,m,c}\mathbf{\Phi}_R\mathbf{F}_i\right)\mathbf{P}_i\bar{\mathbf{1}}_m\right|^2, \\ &|h|_{i,m,e}^2 = \\ &\left|\left(\sqrt{\varepsilon_{i,i,m,e}}\mathbf{w}_{i,i,m,e} + \sqrt{\varepsilon_{i,\mathrm{R},i,m,e}}\mathbf{g}_{i,m,e}\mathbf{\Phi}_R\mathbf{F}_i\right)\mathbf{P}_i\bar{\mathbf{1}}_m\right|^2, \end{aligned} \tag{15}$$

where $\bar{\mathbf{1}}_m = [\ 0\cdots0\ \ 1\ \ 0\cdots0\ ]^T$ represents an $(M \times 1)$ vector, the m-th row of $\bar{\mathbf{1}}_m$ is 1.

Generally speaking, the effective inter-cell interference of the CCU and CEU in cluster m of cell i can be expressed as

$$\begin{aligned} D_{i,m,c} &= \sqrt{\varepsilon_{j,i,m,c}}\mathbf{w}_{j,i,m,c}\mathbf{P}_j\mathbf{1}_M, \\ D_{i,m,e} &= \sqrt{\varepsilon_{j,i,m,e}}\mathbf{w}_{j,i,m,e}\mathbf{P}_j\mathbf{1}_M, \end{aligned} \tag{16}$$

where $\mathbf{1}_M$ represents an all one vector with $(M \times 1)$ elements.

The inter-cluster interference of the CCU and CEU in cluster m of cell i can be expressed as

$$\begin{aligned} B_{i,m,c} &= \sqrt{\varepsilon_{i,i,m,c}}\mathbf{w}_{i,i,m,c}\mathbf{P}_i\bar{\mathbf{0}}_m, \\ B_{i,m,e} &= \sqrt{\varepsilon_{i,i,m,e}}\mathbf{w}_{i,i,m,e}\mathbf{P}_i\bar{\mathbf{0}}_m, \end{aligned} \tag{17}$$

where $\bar{\mathbf{0}}_m = [\ 1\cdots1\ \ 0\ \ 1\cdots1\ ]^T$ represents an $(M \times 1)$ vector containing a zero element in the m-th row.

The BS-RIS-user reflection links for SEB cause additional interference. The CCU and CEU in cluster m of cell i receives interference reflected by STAR-RIS, which can be given by

$$\begin{aligned} Q_{i,m,c} &= \sqrt{\varepsilon_{i,\mathrm{R},i,m,c}}\mathbf{g}_{i,m,c}\mathbf{\Phi}_R\mathbf{F}_i\mathbf{P}_i\bar{\mathbf{0}}_m, \\ Q_{i,m,e} &= \sqrt{\varepsilon_{i,\mathrm{R},i,m,e}}\mathbf{g}_{i,m,e}\mathbf{\Phi}_R\mathbf{F}_i\mathbf{P}_i\bar{\mathbf{0}}_m. \end{aligned} \tag{18}$$

Then, we can express all interferences of CCU and CEU in cluster m of cell i as

$$\begin{aligned} I_{i,m,c} &= D_{i,m,c} + B_{i,m,c} + Q_{i,m,c}, \\ I_{i,m,e} &= D_{i,m,e} + B_{i,m,e} + Q_{i,m,e}. \end{aligned} \tag{19}$$

In the STAR-RIS assisted multiuser MISO-NOMA cellular network, we define the equivalent interferences of CCU and CEU in cluster m of cell i as $\hat{I}_{i,m,c}$ and $\hat{I}_{i,m,e}$. We mitigate the interferences by superimposing them with the STAR-RIS-transmitted signals. Consequently, $\hat{I}_{i,m,c}$ and $\hat{I}_{i,m,e}$ can be represented as

$$\begin{aligned}
\hat{I}_{1,m,c} &= \left|I_{1,m,c} + \sqrt{\varepsilon_{2,\mathrm{R},1,m,c}}\mathbf{g}_{1,m,c}\mathbf{\Phi}_T\mathbf{F}_2\mathbf{P}_2\mathbf{1}_m\right|^2,\\
\hat{I}_{1,m,e} &= \left|I_{1,m,e} + \sqrt{\varepsilon_{2,\mathrm{R},1,m,e}}\mathbf{g}_{1,m,e}\mathbf{\Phi}_T\mathbf{F}_2\mathbf{P}_2\mathbf{1}_m\right|^2,\\
\hat{I}_{2,m,c} &= \left|I_{2,m,c} + \sqrt{\varepsilon_{1,\mathrm{R},2,m,c}}\mathbf{g}_{2,m,c}\mathbf{\Phi}_T\mathbf{F}_1\mathbf{P}_1\mathbf{1}_m\right|^2,\\
\hat{I}_{2,m,e} &= \left|I_{2,m,e} + \sqrt{\varepsilon_{1,\mathrm{R},2,m,e}}\mathbf{g}_{2,m,e}\mathbf{\Phi}_T\mathbf{F}_1\mathbf{P}_1\mathbf{1}_m\right|^2.
\end{aligned} \tag{20}$$

Lemma 1. *We assume that the small-scale fading environments of BS-STAR-RIS and STAR-RIS-user links are strong enough, i.e., $\mathcal{K}_2 = \mathcal{K}_3 \sim \infty$. Hence, to mitigate the interferences of the dual-sided STAR-RIS assisted cellular MISO-NOMA network, the following conditions must be satisfied:*

$$L \geq \max\left\{\Omega_{1,m,c}, \Omega_{1,m,e}, \Omega_{2,m,c}, \Omega_{2,m,e}\right\}. \tag{21}$$

$$\begin{aligned}
\beta_R &< \frac{M\sqrt{d_{1,\mathrm{R}}^{-\alpha_3}}}{M\sqrt{d_{1,\mathrm{R}}^{-\alpha_3}} + (M-1)\sqrt{d_{2,\mathrm{R}}^{-\alpha_3}}},\\
\beta_R &< \frac{M\sqrt{d_{2,\mathrm{R}}^{-\alpha_3}}}{M\sqrt{d_{2,\mathrm{R}}^{-\alpha_3}} + (M-1)\sqrt{d_{1,\mathrm{R}}^{-\alpha_3}}}.
\end{aligned} \tag{22}$$

where

$$\begin{aligned}
\Omega_{1,m,k} &= \frac{(M-1)\sqrt{d_{1,1,m,k}^{-\alpha_2}} + M\sqrt{d_{2,1,m,k}^{-\alpha_1}}}{\left[(1-M)\beta_R\sqrt{d_{1,\mathrm{R}}^{-\alpha_3}} + M\beta_T\sqrt{d_{2,\mathrm{R}}^{-\alpha_3}}\right]\sqrt{d_{\mathrm{R},1,m,k}^{-\alpha_4}}},\\
\Omega_{2,m,k} &= \frac{(M-1)\sqrt{d_{2,2,m,k}^{-\alpha_2}} + M\sqrt{d_{1,2,m,k}^{-\alpha_1}}}{\left[(1-M)\beta_R\sqrt{d_{2,\mathrm{R}}^{-\alpha_3}} + M\beta_T\sqrt{d_{1,\mathrm{R}}^{-\alpha_3}}\right]\sqrt{d_{\mathrm{R},2,m,k}^{-\alpha_4}}}.
\end{aligned} \tag{23}$$

Proof: To eliminate inter-cluster interference, it is necessary to satisfy

$$\begin{aligned}
(M-1)\sqrt{d_{1,1,m,k}^{-\alpha_2}} &\leq \beta_T LM\sqrt{d_{2,\mathrm{R}}^{-\alpha_3}d_{\mathrm{R},1,m,k}^{-\alpha_4}},\\
(M-1)\sqrt{d_{2,2,m,k}^{-\alpha_2}} &\leq \beta_T LM\sqrt{d_{1,\mathrm{R}}^{-\alpha_3}d_{\mathrm{R},2,m,k}^{-\alpha_4}}.
\end{aligned} \tag{24}$$

Similarly, to eliminate the inter-cell interference, it is necessary to satisfy

$$\begin{aligned}
M\sqrt{d_{2,1,m,k}^{-\alpha_1}} &\leq \beta_T LM\sqrt{d_{2,\mathrm{R}}^{-\alpha_3}d_{\mathrm{R},1,m,k}^{-\alpha_4}},\\
M\sqrt{d_{1,2,m,k}^{-\alpha_1}} &\leq \beta_T LM\sqrt{d_{1,\mathrm{R}}^{-\alpha_3}d_{\mathrm{R},2,m,k}^{-\alpha_4}}.
\end{aligned} \tag{25}$$

To eliminate the interference caused by SEB-sector, the following conditions need to be met

$$\begin{aligned}
\beta_R L(M-1)\sqrt{d_{1,\mathrm{R}}^{-\alpha_3}d_{\mathrm{R},1,m,k}^{-\alpha_4}} &\leq \beta_T LM\sqrt{d_{2,\mathrm{R}}^{-\alpha_3}d_{\mathrm{R},1,m,k}^{-\alpha_4}},\\
\beta_R L(M-1)\sqrt{d_{2,\mathrm{R}}^{-\alpha_3}d_{\mathrm{R},2,m,k}^{-\alpha_4}} &\leq \beta_T LM\sqrt{d_{1,\mathrm{R}}^{-\alpha_3}d_{\mathrm{R},2,m,k}^{-\alpha_4}}.
\end{aligned} \tag{26}$$

Combining (24)*,* (25) *and* (26)*, the required number of STAR-RIS elements for interference mitigation needs to satisfy*

$$\begin{aligned}
&(M-1)\sqrt{d_{1,1,m,k}^{-\alpha_2}} + M\sqrt{d_{2,1,m,k}^{-\alpha_1}} +\\
&\beta_R L(M-1)\sqrt{d_{1,\mathrm{R}}^{-\alpha_3}d_{\mathrm{R},1,m,k}^{-\alpha_4}} \leq \beta_T LM\sqrt{d_{2,\mathrm{R}}^{-\alpha_3}d_{\mathrm{R},1,m,k}^{-\alpha_4}},\\
&(M-1)\sqrt{d_{2,2,m,k}^{-\alpha_2}} + M\sqrt{d_{1,2,m,k}^{-\alpha_1}} +\\
&\beta_R L(M-1)\sqrt{d_{2,\mathrm{R}}^{-\alpha_3}d_{\mathrm{R},2,m,k}^{-\alpha_4}} \leq \beta_T LM\sqrt{d_{1,\mathrm{R}}^{-\alpha_3}d_{\mathrm{R},2,m,k}^{-\alpha_4}}.
\end{aligned} \tag{27}$$

After some algebraic operations, Eq. (27) *can be rewritten as*

$$\begin{aligned}
L &\geq \frac{(M-1)\sqrt{d_{1,1,m,k}^{-\alpha_2}} + M\sqrt{d_{2,1,m,k}^{-\alpha_1}}}{\left[(1-M)\beta_R\sqrt{d_{1,\mathrm{R}}^{-\alpha_3}} + M\beta_T\sqrt{d_{2,\mathrm{R}}^{-\alpha_3}}\right]\sqrt{d_{\mathrm{R},1,m,k}^{-\alpha_4}}},\\
L &\geq \frac{(M-1)\sqrt{d_{2,2,m,k}^{-\alpha_2}} + M\sqrt{d_{1,2,m,k}^{-\alpha_1}}}{\left[(1-M)\beta_R\sqrt{d_{2,\mathrm{R}}^{-\alpha_3}} + M\beta_T\sqrt{d_{1,\mathrm{R}}^{-\alpha_3}}\right]\sqrt{d_{\mathrm{R},2,m,k}^{-\alpha_4}}},
\end{aligned} \tag{28}$$

where

$$\begin{aligned}
(1-M)\beta_R\sqrt{d_{1,\mathrm{R}}^{-\alpha_3}} + M\beta_T\sqrt{d_{2,\mathrm{R}}^{-\alpha_3}} > 0,\\
(1-M)\beta_R\sqrt{d_{2,\mathrm{R}}^{-\alpha_3}} + M\beta_T\sqrt{d_{1,\mathrm{R}}^{-\alpha_3}} > 0.
\end{aligned} \tag{29}$$

After some algebraic manipulations, the results in (21) *and* (22) *can be deduced, completing the proof of* **Lemma 1**. ■

E. Problem Formulation

Based on the expression of the effective channel gains in (15) and the equivalent interferences in (20), we can express the SINR of CCU and CEU in cluster m of cell i as

$$\begin{aligned}
SINR_{i,m,c} &= \frac{|h|_{i,m,c}^2 p_i \alpha_c^2}{\hat{I}_{i,m,c}p_i + N_0^{i,m,c}}\\
SINR_{i,m,e} &= \frac{|h|_{i,m,e}^2 p_i \alpha_e^2}{|h|_{i,m,e}^2 p_i \alpha_c^2 + \hat{I}_{i,m,e}p_i + N_0^{i,m,e}}.
\end{aligned} \tag{30}$$

By jointly optimizing the power allocation factors of NOMA users, the precoding matrix of BSs, as well as the reflection and transmission phase shifts at the STAR-RIS, we can formulate the spectral efficiency maximization problem as

$$\begin{aligned}
\max_{\mathbf{\Phi}_R,\mathbf{\Phi}_T,\mathbf{P}_1,\mathbf{P}_2,\alpha_c,\alpha_e} \quad & \sum_{i=1}^{2}\sum_{m=1}^{M}(\hat{R}_{i,m,c} + \hat{R}_{i,m,e})\\
\text{s.t.} \quad & C1: \theta_{R,l} \in [0, 2\pi), \forall l = 1, 2, \ldots, L,\\
& C2: \theta_{T,l} \in [0, 2\pi), \forall l = 1, 2, \ldots, L,\\
& C3: \beta_R^2 + \beta_T^2 = 1,\\
& C4: \alpha_c^2 + \alpha_e^2 = 1,\\
& C5: \hat{R}_{i,m,c} \geq R_{i,m,c}^*, \hat{R}_{i,m,e} \geq R_{i,m,e}^*,\\
& C6: \|\mathbf{P}_1\|_2^2 \leq 1, \|\mathbf{P}_2\|_2^2 \leq 1.
\end{aligned} \tag{31}$$

where $\hat{R}_{i,m,c} = \log_2(1 + SINR_{i,m,c})$ and $\hat{R}_{i,m,e} = \log_2(1 + SINR_{i,m,e})$ represent the achievable rates of CCU and CEU, respectively. $R_{i,m,c}^*$ and $R_{i,m,e}^*$ are the target data rates of CCU and CEU, respectively. $C1$, $C2$ and $C3$ are the constraint

conditions of the dual-sided STAR-RIS array, $C4$ is the constraint condition of the power allocation factors, $C5$ is the constraint condition of the achievable rate, $C6$ is the constraint condition of the precoding matrix.

Based on the proposed SSEIM design, we aim at maximizing the desired signals and minimizing the interference signals. We can decompose the optimization problem in (31) into three subproblems: the SEB-sector, the IMB-sector and the power allocation sector. Since the SEB-sector can cause additional interference, it should be designed first. We first focus on maximizing the effective channel power gain by jointly optimizing the reflection phase shifts of each STAR-RIS element and the precoding matrix of BSs as follows:

$$\begin{aligned} \max_{\mathbf{\Phi}_R,\mathbf{P}_1,\mathbf{P}_2} \quad & \sum_{i=1}^{2}\sum_{m=1}^{M}\left(|h|_{i,m,c}^2+|h|_{i,m,e}^2\right) \\ \text{s.t.} \quad & C1, C6. \end{aligned} \tag{32}$$

Next, the equivalent interference can be minimized by optimizing the transmission phase shifts of each STAR-RIS elements as follows:

$$\begin{aligned} \min_{\mathbf{\Phi}_T} \quad & \sum_{i=1}^{2}\sum_{m=1}^{M}(\hat{I}_{i,m,c}+\hat{I}_{i,m,e}) \\ \text{s.t.} \quad & C2. \end{aligned} \tag{33}$$

Finally, to guarantee users' fairness, the optimization of power allocation factors for NOMA users is conducted based on the target data rate and CSI. We develop the optimization problem as:

$$\begin{aligned} \max_{\alpha_c,\alpha_e} \quad & \sum_{i=1}^{2}\sum_{m=1}^{M}(\hat{R}_{i,m,c}+\hat{R}_{i,m,e}) \\ \text{s.t.} \quad & C4, C5. \end{aligned} \tag{34}$$

III. Signal Enhancement Design

In this section, we first pay attention to the SEB-sector. Similar to equation (30), we can express the SNR of CCU and CEU in cluster m of cell i as

$$\begin{aligned} SNR_{i,m,c}&=\frac{|h|_{i,m,c}^2 p_i\alpha_c^2}{N_0^{i,m,c}} \\ SNR_{i,m,e}&=\frac{|h|_{i,m,e}^2 p_i\alpha_e^2}{|h|_{i,m,e}^2 p_i\alpha_c^2+N_0^{i,m,e}}. \end{aligned} \tag{35}$$

By utilizing the high SNR approximation in [37], the SNR of CEU in the m-th cluster is further expressed as

$$SNR_{i,m,e}\approx\frac{\alpha_e^2}{\alpha_c^2}, \tag{36}$$

which is a constant. It shows that the effective channel power gain of CCU plays a major role in the SEB-sector. Therefore, the optimization problem (32) can be transformed into

$$\begin{aligned} \max_{\mathbf{\Phi}_R,\mathbf{P}_1,\mathbf{P}_2} \quad & \sum_{m=1}^{M}\left(|h|_{1,m,c}^2+|h|_{2,m,c}^2\right) \\ \text{s.t.} \quad & C1, C6. \end{aligned} \tag{37}$$

To enhance the effective channel power gain, the MRT technique is employed to jointly optimize the precoding matrix $\mathbf{P}_i$ and the phase shifts of dual-sided STAR-RIS [38], [39]. As defined by equation (15) for $|h|_{i,m,c}^2$, the MRT beamforming vector of the m-th cluster of BS i is a $(M\times 1)$ vector, which is specified as follows:

$$\hat{\mathbf{p}}_{i,m}^H=\frac{\left(\sqrt{\varepsilon_{i,i,m,c}}\mathbf{w}_{i,i,m,c}+\sqrt{\varepsilon_{i,\mathrm{R},i,m,c}}\mathbf{g}_{i,m,c}\mathbf{\Phi}_R\mathbf{F}_i\right)}{\left\|\sqrt{\varepsilon_{i,i,m,c}}\mathbf{w}_{i,i,m,c}+\sqrt{\varepsilon_{i,\mathrm{R},i,m,c}}\mathbf{g}_{i,m,c}\mathbf{\Phi}_R\mathbf{F}_i\right\|_2}. \tag{38}$$

We define an $(L\times 1)$ effective STAR-RIS reflection vector $\mathbf{\Psi}_R=[\phi_{R,1},\cdots,\phi_{R,L}]^H=\left[e^{j'\theta_{R,1}},\cdots,e^{j'\theta_{R,L}}\right]^H$. Concurrently, the effective channel power gains of the CCU can be reformulated as

$$\begin{aligned} |h|_{1,m,c}^2&=\left|\left(\sqrt{\varepsilon_{1,1,m,c}}\mathbf{w}_{1,1,m,c}+\mathbf{\Psi}_R^H\tilde{\mathbf{a}}_{1,m}\right)\hat{\mathbf{p}}_{1,m}\right|^2, \\ |h|_{2,m,c}^2&=\left|\left(\sqrt{\varepsilon_{2,2,m,c}}\mathbf{w}_{2,2,m,c}+\mathbf{\Psi}_R^H\tilde{\mathbf{a}}_{2,m}\right)\hat{\mathbf{p}}_{2,m}\right|^2, \end{aligned} \tag{39}$$

where $\tilde{\mathbf{a}}_{i,m}=\beta_R\sqrt{\varepsilon_{i,R,i,m,c}}\mathrm{diag}(\mathbf{g}_{i,m,c})\mathbf{F}_i$, $\hat{\mathbf{p}}_{i,m}$ in (38) can be further transformed into

$$\hat{\mathbf{p}}_{i,m}^H=\frac{\sqrt{\varepsilon_{i,i,m,c}}\mathbf{w}_{i,i,m,c}+\mathbf{\Psi}_R^H\tilde{\mathbf{a}}_{i,m}}{\left\|\sqrt{\varepsilon_{i,i,m,c}}\mathbf{w}_{i,i,m,c}+\mathbf{\Psi}_R^H\tilde{\mathbf{a}}_{i,m}\right\|_2}. \tag{40}$$

The objective function $f(\mathbf{\Psi}_R)$ is given by

$$f(\mathbf{\Psi}_R)=-\sum_{i=1}^{2}\sum_{m=1}^{M}\Lambda_{i,m}\Lambda_{i,m}^H, \tag{41}$$

where $\Lambda_{i,m}=\sqrt{\varepsilon_{i,i,m,c}}\mathbf{w}_{i,i,m,c}+\mathbf{\Psi}_R^H\tilde{\mathbf{a}}_{i,m}$.

The constraint condition $\theta_{R,l}\in[0,2\pi)$ can be expressed in terms of the modulus of a complex exponential, where $|\phi_{R,l}|=\left|e^{j'\theta_{R,l}}\right|=1$. The formulation states that the magnitude of the complex number, represented as the exponential of a purely imaginary number $j'\theta_{R,l}$, is equal to one. We can reframe the problem presented in (37) accordingly:

$$\begin{aligned} \min_{\mathbf{\Psi}_R} \quad & f(\mathbf{\Psi}_R) \\ \text{s.t.} \quad & C7: |\phi_{R,l}|=1, \forall l=1,\ldots,L. \end{aligned} \tag{42}$$

We can see that the objective function $f(\mathbf{\Psi}_R)$ is continuous and differentiable, the constraint condition is intrinsically non-convex. The optimization variables $\mathbf{\Psi}_R(\phi)=[\phi_{R,1},\cdots,\phi_{R,L}]^H$ are on an L-dimensional Riemannian submanifold $\mathcal{M}_{cc}^L$, which can be defined by

$$\mathcal{M}_{cc}^L=\{\mathbf{\Psi}_R\in\mathcal{C}^L\,|\phi_{R,1}^*\phi_{R,1}=\phi_{R,l}^*\phi_{R,l}=\phi_{R,L}^*\phi_{R,L}=1\}, \tag{43}$$

where $\mathcal{C}^L$ is a L-dimensional complex space [40].

We introduce the proposed RCG algorithm to solve the above optimization problem, which can effectively deal with non-convex optimization problems [15], [40]–[42]. The following are three basic steps of the proposed RCG algorithm:

1) Calculate Riemannian Gradient: Riemannian gradient is the fastest growing direction (tangent vector) of the objective function, which can be calculated by the orthogonal projection of the Euclidean gradient $\nabla f(\mathbf{\Psi}_R)$ as follows:

$$\mathrm{grad}f=\nabla f(\mathbf{\Psi}_R)-\mathrm{Re}\{\nabla f(\mathbf{\Psi}_R)\circ\mathbf{\Psi}_R^*\}\circ\mathbf{\Psi}_R, \tag{44}$$

where $f(\mathbf{\Psi}_R)$ is the Euclidean gradient, which is calculated

as

$$\nabla f(\mathbf{\Psi}_R) = - \sum_{m=1}^{M} 2\left[\tilde{\mathbf{a}}_{1,m}\tilde{\mathbf{a}}_{1,m}^H\mathbf{\Psi}_R + \tilde{\mathbf{a}}_{1,m}\big(\sqrt{\varepsilon_{1,1,m,c}}\mathbf{w}_{1,1,m,c}\big)^H\right] - \sum_{m=1}^{M} 2\left[\tilde{\mathbf{a}}_{2,m}\tilde{\mathbf{a}}_{2,m}^H\mathbf{\Psi}_R + \tilde{\mathbf{a}}_{2,m}\big(\sqrt{\varepsilon_{2,2,m,c}}\mathbf{w}_{2,2,m,c}\big)^H\right]. \tag{45}$$

2) Search Direction: For the conjugate gradient (CG) method on manifolds, the tangent vector conjugate to $\mathrm{grad}f$ is our search direction, which is formulated as

$$d = -\mathrm{grad}f + \tau\Xi(\bar{d}), \tag{46}$$

where τ is the conjugate gradient update parameter, which changes with the number of iterations k. $\bar{d}$ denotes the previous search direction, and the vector transport function $\Xi(\bullet)$ can be given by

$$\Xi(d) = d - \mathrm{Re}\{d \circ \mathbf{\Psi}_R^*\} \circ \mathbf{\Psi}_R. \tag{47}$$

3) Retraction: In order to determine the next point on the complex circle manifold, we project the tangent vector back to the manifold itself, which is called retraction, and it can be represented as

$$(\mathbf{\Psi}_R)_k \leftarrow \frac{(\mathbf{\Psi}_R + \nu d)_k}{|(\mathbf{\Psi}_R + \nu d)_k|}, \tag{48}$$

where ν is the Armijo step size.

We initialize $\mathbf{\Psi}_{R,0}$ by using a heuristic method [41]. By relaxing the constraint condition $C7$ to $\|\mathbf{\Psi}_R\|_2^2 = L$, the optimal solution of problem (42) can be written as

$$\hat{\mathbf{\Psi}}_R^H = \frac{\sqrt{L}\sum_{i=1}^{2}\sum_{m=1}^{M}\left(-\sqrt{\varepsilon_{i,i,m,c}}\mathbf{w}_{i,i,m,c}(\tilde{\mathbf{a}}_{i,m})^+\right)}{2M}, \tag{49}$$

where $(\tilde{\mathbf{a}}_{i,m})^+$ is the pseudo-inverse matrix of $\tilde{\mathbf{a}}_{i,m}$.

By utilizing the proposed RCG algorithm, an optimal solution of $\mathbf{\Psi}_R$ for maximizing the effective channel power gain can be obtained. We can formulate the MRT precoding matrix according to (40), which can be rewritten as $\mathbf{P}_i = (\hat{\mathbf{p}}_{i,1}, ..., \hat{\mathbf{p}}_{i,M})$. Thus, the solution of optimization problems (42) and (32) is obtained. The detailed process of RCG algorithm is shown in **Algorithm 1**, where the initial point $\mathbf{\Psi}_{R,0}$ is given by $\hat{\mathbf{\Psi}}_R \Big/ \left|\hat{\mathbf{\Psi}}_R\right|$.

Algorithm 1 The proposed RCG algorithm

Require: L, M, $\sqrt{\varepsilon_{1,1,m,c}}\mathbf{w}_{1,1,m,c}$, $\sqrt{\varepsilon_{2,2,m,c}}\mathbf{w}_{2,2,m,c}$, $\tilde{\mathbf{a}}_{1,m}$, $\tilde{\mathbf{a}}_{2,m}$

1: Initialize $k = 0$, $\mathbf{\Psi}_{R,0} \in \mathcal{M}_{cc}^L$, $\mathrm{d}_0 = \mathrm{grad}f(\mathbf{\Psi}_{R,0})$.
2: **while** not converged **do**
3: Choose Armiji step size ν_k.
4: Calculate $\mathbf{\Psi}_{R,k}$ according to (48): $\mathbf{\Psi}_{R,k+1} = \frac{\mathbf{\Psi}_{R,k}+\nu_k d_k}{|\mathbf{\Psi}_{R,k}+\nu_k d_k|}$.
5: Based on (44) and (45), compute the Riemannian gradient: $g_{k+1} = \mathrm{grad}f(\mathbf{\Psi}_{R,k+1})$.
6: Determine vector transports $\Xi(g_k)$ and $\Xi(d_k)$ of gradient g_k and conjugate direction d_k according to (47).
7: Compute conjugate gradient update parameters τ: $\tau = \frac{g_{k+1}^H g_{k+1}}{\bar{g}_k^H \bar{g}_k}$.
8: Calculate the search direction d_{k+1} by (46).
9: Update $k \leftarrow k+1$.
10: **end while**
11: **return** $\mathbf{\Psi}_R = \mathbf{\Psi}_{R,k+1}$

IV. Interference Mitigation Design

A. Interference mitigation

We then optimize the transmission phase shifts of STAR-RIS elements to mitigate the interferences. In the proposed SSEIM design, the $(L \times 1)$ effective STAR-RIS transmission vector can be defined by

$$\mathbf{\Psi}_T(\phi) = [\phi_{T,1}, \cdots, \phi_{T,L}]^H = \left[e^{j'\theta_{T,1}}, \cdots, e^{j'\theta_{T,L}}\right]^H. \tag{50}$$

Then, the interferences in (20) can be rewritten as

$$\begin{aligned}\hat{I}_{i,m,c} &= \left|I_{i,m,c} + \mathbf{\Psi}_T^H\mathbf{V}_{i,m,c}\right|^2,\\ \hat{I}_{i,m,e} &= \left|I_{i,m,e} + \mathbf{\Psi}_T^H\mathbf{V}_{i,m,e}\right|^2,\end{aligned} \tag{51}$$

where

$$\begin{aligned}\mathbf{V}_{i,m,c} &= \beta_T\sqrt{\varepsilon_{j,\mathrm{R},i,m,c}}\mathrm{diag}(\mathbf{g}_{i,m,c})\mathbf{F}_j\mathbf{P}_j\mathbf{1}_M,\\ \mathbf{V}_{i,m,e} &= \beta_T\sqrt{\varepsilon_{j,\mathrm{R},i,m,e}}\mathrm{diag}(\mathbf{g}_{i,m,e})\mathbf{F}_j\mathbf{P}_j\mathbf{1}_M.\end{aligned} \tag{52}$$

The objective function for IMB-sector is further reformulated as

$$y(\mathbf{\Psi}_T) = \sum_{m=1}^{M}(\hat{I}_{1,m,c} + \hat{I}_{1,m,e}) + \sum_{m=1}^{M}(\hat{I}_{2,m,c} + \hat{I}_{2,m,e}), \tag{53}$$

which is continuous and differentiable. The constraint condition $\theta_{T,l} \in [0, 2\pi)$ can be equivalently expressed as the modulus of a complex exponential, where $|\phi_{T,l}| = \left|e^{j'\theta_{T,l}}\right| = 1$. The phase shifts of STAR-RIS elements are confined to the unit circle in the complex plane. Therefore, the optimization problem in (33) is simplified as

$$\begin{aligned}\min_{\mathbf{\Psi}_T} \quad & y(\mathbf{\Psi}_T)\\ \text{s.t.} \quad & C8: |\phi_{T,l}| = 1, \quad \forall l = 1, \ldots, L.\end{aligned} \tag{54}$$

By relaxing the constraint condition $C8$ to $\|\mathbf{\Psi}_T\|_2^2 = L$, the optimal solution is given by

$$\hat{\mathbf{\Psi}}_T^H = \frac{\sqrt{L}\sum_{i=1}^{2}\sum_{m=1}^{M}\left(-I_{i,m,c}(\mathbf{V}_{i,m,c})^+ - I_{i,m,e}(\mathbf{V}_{i,m,e})^+\right)}{2M}. \tag{55}$$

We still solve $\mathbf{\Psi}_T$ by the proposed RCG algorithm. The initial point $\mathbf{\Psi}_{T,0} = \hat{\mathbf{\Psi}}_T \Big/ \left|\hat{\mathbf{\Psi}}_T\right|$. The Riemannian gradient, search direction and retraction are all calculated by using the similar method in (44), (46) and (48). We define $\nabla y(\mathbf{\Psi}_T)$ as the Euclidean gradient of $y(\mathbf{\Psi}_T)$, which can be given by

$$\nabla y(\mathbf{\Psi}_T) = \sum_{i=1}^{2}\sum_{m=1}^{M} 2\left(\mathbf{V}_{i,m,c}\mathbf{V}_{i,m,c}^H\mathbf{\Psi}_T + \mathbf{V}_{i,m,c}(I_{i,m,c})^*\right) + \sum_{i=1}^{2}\sum_{m=1}^{M} 2\left(\mathbf{V}_{i,m,e}\mathbf{V}_{i,m,e}^H\mathbf{\Psi}_T + \mathbf{V}_{i,m,e}(I_{i,m,e})^*\right). \tag{56}$$

B. User fairness analysis

After appropriately adjusting the precoding matrix of BSs, the phase shifts of STAR-RIS elements, we can obtain stronger channel gain and weaker interference. By utilizing the high SNR approximation in [37], the achievable rate of CEU in the m-th cluster is further expressed as

$$\hat{R}_{i,m,e} \approx \log_2(1+\frac{\alpha_e^2}{\alpha_c^2}). \tag{57}$$

Adopting the fixed power allocation, when the power allocation factor of CCU reaches its maximum value, i.e. $\alpha_c = 1$ and $\alpha_e = 0$, the performance of the system is optimal. To ensure user fairness, it is necessary to dynamically adjust the power allocation factors based on the target rate of the CEU, i.e. $\hat{R}_{i,m,e} = R^*_{i,m,e}$. After algebraic transformation, the power allocation factors for CCU and CEU are obtained as follows:

$$\alpha_e^2 = \frac{2^{R^*_{i,m,e}}-1}{2^{R^*_{i,m,e}}} \quad \text{and} \quad \alpha_c^2 = 1-\alpha_e^2. \tag{58}$$

At this stage, the interference is effectively mitigated, the desired signal is enhanced, user fairness is ensured. All three sub-optimization problems have been resolved, yielding the solution to the optimization problem in (31). The detailed procedure is presented in **Algorithm 2**.

Algorithm 2 The proposed LSEM algorithm

Require: L, M, the target rate $R^*_{i,m,e}$,
the large-scale fading $\sqrt{\varepsilon_{1,1,m,c}}$, $\sqrt{\varepsilon_{2,2,m,c}}$, $\sqrt{\varepsilon_{1,1,m,e}}$, $\sqrt{\varepsilon_{2,2,m,e}}$, $\sqrt{\varepsilon_{1,2,m,c}}$, $\sqrt{\varepsilon_{2,1,m,c}}$, $\sqrt{\varepsilon_{1,2,m,e}}$, $\sqrt{\varepsilon_{2,1,m,e}}$, $\sqrt{\varepsilon_{1,\mathrm{R},1,m,c}}$, $\sqrt{\varepsilon_{2,\mathrm{R},2,m,c}}$, $\sqrt{\varepsilon_{1,\mathrm{R},1,m,e}}$, $\sqrt{\varepsilon_{2,\mathrm{R},2,m,e}}$,
the small-scale fading channel matrix $\mathbf{w}_{1,1,m,c}$, $\mathbf{w}_{2,2,m,c}$, $\mathbf{w}_{1,1,m,e}$, $\mathbf{w}_{2,2,m,e}$, $\mathbf{w}_{1,2,m,c}$, $\mathbf{w}_{2,1,m,c}$, $\mathbf{w}_{1,2,m,e}$, $\mathbf{w}_{2,1,m,e}$, $\mathbf{g}_{1,m,c}$, $\mathbf{g}_{2,m,c}$, $\mathbf{g}_{1,m,e}$, $\mathbf{g}_{2,m,e}$, $\mathbf{F}_1$, $\mathbf{F}_2$,
the reflected amplitude coefficient β_R and the transmitted amplitude coefficient β_T.

1: Compute $\tilde{\mathbf{a}}_{1,m}$ and $\tilde{\mathbf{a}}_{2,m}$,
2: Initialize $k=0, \mathbf{\Psi}_{R,0} \in \mathcal{M}_{cc}^L$,
calculate $\mathrm{d}_0 = \mathrm{grad} f(\mathbf{\Psi}_{R,0})$,
3: Calculate $\mathbf{\Psi}_R$ based on **Algorithm 1**.
4: Compute the MRT beamforming vector $\hat{\mathbf{p}}_{i,m}$ based on (40),
5: Calculate the MRT precoding matrix $\mathbf{P}_i = (\hat{\mathbf{p}}_{i,1},...,\hat{\mathbf{p}}_{i,M})$.
6: Compute the effective inter-cell interference $D_{1,m,c}$, $D_{1,m,e}$, $D_{2,m,c}$, $D_{2,m,e}$,
7: Calculate the inter-cluster interference $B_{1,m,c}$, $B_{1,m,e}$, $B_{2,m,c}$, $B_{2,m,e}$,
8: Compute the interference reflected by STAR-RIS $Q_{1,m,c}$, $Q_{1,m,e}$, $Q_{2,m,c}$, $Q_{2,m,e}$,
9: Calculate all interference $I_{1,m,c}$,$I_{1,m,e}$,$I_{2,m,c}$,$I_{2,m,e}$ by (19).
10: Compute $\mathbf{V}_{1,m,c}$,$\mathbf{V}_{1,m,e}$,$\mathbf{V}_{2,m,c}$,$\mathbf{V}_{2,m,e}$ by (52),
11: Initialize $\hat{k}=0, \mathbf{\Psi}_{T,0} \in \mathcal{M}_{cc}^L$,
calculate $\hat{\mathrm{d}}_0 = \mathrm{grad} y(\mathbf{\Psi}_{T,0})$,
12: Calculate $\mathbf{\Psi}_T$ based on **Algorithm 1**.
13: Calculate the power allocation factors α_c^2 and α_e^2 by (58).
14: **return** $\mathbf{\Psi}_R$, $\mathbf{\Psi}_T$, $\mathbf{P}_1$, $\mathbf{P}_2$, α_c^2, α_e^2.

TABLE I:
Compare the computational complexity of the proposed RCG algorithm with the majorization-minimization algorithm and the semidefinite relaxation algorithm.

Mode	Computational Complexity
semidefinite relaxation algorithm [41]	$O((L+1)^6)$
majorization-minimization algorithm [46]	$O(L^3)$
the proposed RCG algorithm	$O(L^{1.5})$

Based on **Algorithm 2**, we can calculate the achievable rate of all users. Furthermore, the SE of the cellular MISO-NOMA networks can be computed as follows

$$SE_i = \sum_{m=1}^{M}\left(\hat{R}_{i,m,c}+\hat{R}_{i,m,e}\right). \tag{59}$$

Since L passive STAR-RIS elements serve two cells at the same time, only STAR-RIS phase shifter needs power supply [43], [44], and the total dissipation power in two cells can be modeled as

$$P_e = 2(p\varepsilon_b + 2MP_{\mathrm{U}} + P_{\mathrm{B,s}}) + LP_L, \tag{60}$$

where p is the transmit power of BS, ε_b is the power amplifier efficiency of BS. $2P_{\mathrm{U}}$ is the total power consumption at CCU and CEU in cluster m of cell i, the circuit power consumption at the BS is $P_{\mathrm{B,s}}$. P_L is the circuit power consumption of each STAR-RIS controller. Then, we can express the EE as $EE = \frac{SE_1+SE_2}{P_e}$.

C. Analysis of algorithm complexity and convergence

We propose a LSEM algorithm that utilizes two consecutive RCG algorithms, which effectively address the optimization problem in (31). Based on Theorem 4.3.1 cited in [45], it is demonstrated that both **Algorithm 1** and **Algorithm 2** converge to a critical point. Table I provides a comparative analysis of computational complexities. In the worst-case scenario, the computational complexity of the proposed RCG algorithm is $O(L^{1.5})$. In comparison, **Algorithm 1** exhibits substantially lower computational complexity than both the semidefinite relaxation and majorization-minimization algorithms.

V. Numerical Results

To validate the effectiveness of the proposed STAR-RIS assisted SSEIM design, numerical results are presented in this section. The simulation parameters are shown in Table II. Specifically, the direct link from BS to users is complex with many obstacles, resulting in the relatively large path loss exponent α_1 and α_2. In order to improve the performance of cellular MISO-NOMA system, the signal can propagate more smoothly with fewer surrounding obstacles in the STAR-RIS link, thereby resulting in smaller α_3 and α_4 [47]. Accordingly, the direct link has abundant multipath signals, which results in a very small Rician factor $\mathcal{K}_1$, whereas the larger Rician factor

of STAR-RIS $\mathcal{K}_2$ and $\mathcal{K}_3$ [21]. All the simulation results are averaged over 2×10^3 independent small-scale fading channel realizations.

TABLE II: Simulation parameters.

Target rate of the CEU	$R^*_{i,m,e} = 1.3$ bits/s/Hz [48]
Rician fading factor	$\mathcal{K}_1 = 1$, $\mathcal{K}_2 = 2$, $\mathcal{K}_3 = 3$ [21]
Distances	$d_{i,i,m,c} = 30$m, $d_{i,i,m,e} = 60$m, $d_{i,j,m,c} = 120$m, $d_{i,j,m,e} = 90$m, $d_{i,R} = 70$m, $d_{\mathrm{R},j,m,c} = 50$m, $d_{\mathrm{R},j,m,e} = 15$m
Path loss exponent	$\alpha_1 = \alpha_2 = 3.7$, $\alpha_3 = 3$, $\alpha_{4,c} = 2.5$, $\alpha_{4,e} = 2.3$ [47]
Correlation coefficients	$r_d = 0, r_R = 0.5, r_{R,u} = 0.6$
Horizontal or vertical AoA/AoD	$\vartheta_R = \frac{\pi}{4}, \vartheta_{R,u,c} = \frac{\pi}{3}, \vartheta_{R,u,e} = \frac{\pi}{6}$
Number of STAR-RIS elements	$L = L_v L_h = 32 \times 32 = 1024$
Carrier frequency	$f = 2.4$ GHz
Transmission bandwidth	$BW = 1$ MHz
AWGN power	$\sigma^2 = -174 + 10\log_{10}(BW)$ dBm
Number of transmit antennas	$M = 2$

In order to better illustrate the performance gain of our proposed STAR-RIS assisted SSEIM design, we also evaluate the performance of the following 4 baseline schemes:

- **Baseline 1 (RIS-aided SEB design):** We set $\beta_R = 1$ and $\beta_T = 0$. At this point, the STAR-RIS becomes a conventional reflecting-only RIS. In the cellular communication system, only the reflection of RIS can be utilized to enhance the desired signal.
- **Baseline 2 (RIS-aided IMB design):** We set $\beta_R = 0$ and $\beta_T = 1$. At this point, the STAR-RIS becomes a conventional transmitting-only RIS. In the cellular communication system, only the transmission of RIS can be utilized to mitigate the interferences.
- **Baseline 3 (random STAR-RIS):** The transmission and reflection phase shifts of STAR-RIS are obtained through random initialization.
- **Baseline 4 (without STAR-RIS):** In this case, there is no STAR-RIS in the MISO-NOMA cellular networks.

To better demonstrate the performance advantages of MRT precoding matrix, the following two precoding strategies are introduced:

- **Identity precoding matrix:** The signals are transmitted without any precoding adjustments.
- **ZF precoding matrix:** ZF precoding ensures that the signals intended for different users are orthogonal, which is designed to eliminate inter-user interference [49], [50].

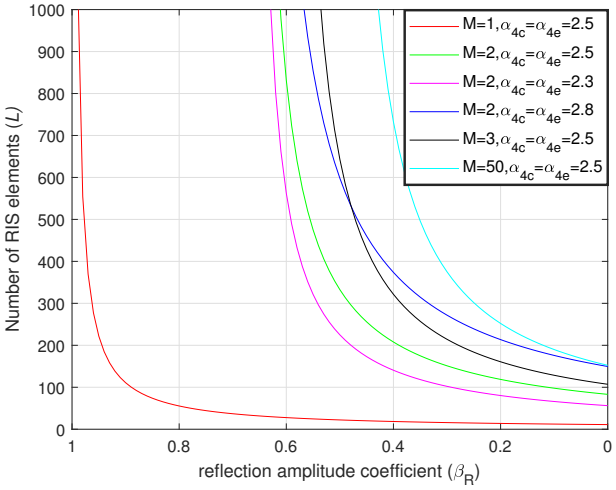

Fig. 2: Minimal required number of STAR-RIS elements for interference mitigation.

1) Minimal required number of STAR-RIS elements:

We study the minimal required number of STAR-RIS elements versus reflection amplitude coefficient with different numbers of TAs in Fig. 2, where the theoretical expression is derived in **Lemma 1**. As the reflection amplitude coefficient increases, we observe that the minimal required number increases rapidly to infinity. Besides, there is an upper bound of the reflection coefficient, which depends on the number of TAs. As the number of TAs increases, the upper bound value decreases. When the number of TAs is infinite, the upper bound is close to 0.5. When the reflection amplitude coefficient reaches the upper bound, no matter how many STAR-RIS elements are deployed, the interferences cannot be completely eliminated.

2) Convergence of the proposed RCG algorithm:

Fig. 3 presents a convergence analysis of the proposed RCG algorithm. Specifically, Fig. 3(a) illustrates the algorithm convergence when applied to solving the STAR-RIS reflection vector $\mathbf{\Psi}_R$, while Fig. 3(b) demonstrates the convergence for the effective STAR-RIS transmission vector $\mathbf{\Psi}_T$. The x-axis denotes the number of iterations, the y-axis represents the number of STAR-RIS elements, and the z-axis displays the Riemannian gradient of the objective function. The algorithm is considered to have converged when the Riemannian gradient falls below 10^{-6}.

As the number of STAR-RIS elements increases, the required number of iterations for algorithm convergence increases. As the reflection power coefficient β_R^2 of STAR-RIS increases, the required number of iterations for convergence of the RCG algorithm solving the STAR-RIS reflection vector increases. In the process of optimizing $\mathbf{\Psi}_R$, the gradient of the objective function initially increases and subsequently decreases. Consequently, the algorithm convergence for SEB sector demands a higher number of iterations. Fig. 3 illustrates that algorithm convergence for the IMB sector requires about 10 iterations, while the SEB sector necessitates between 10 and 20 iterations to achieve convergence. It is associated

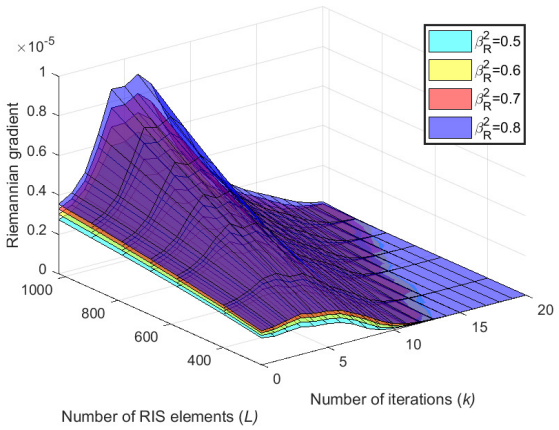

(a) SEB sector

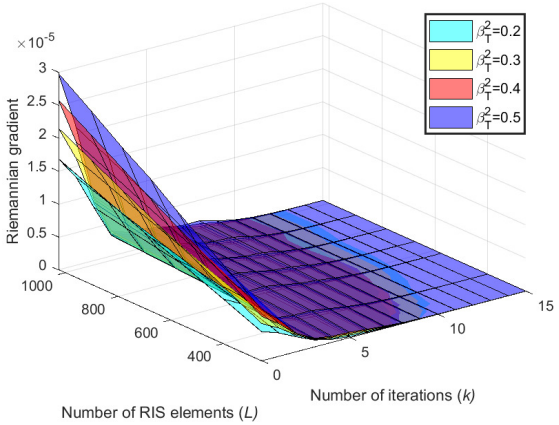

(b) IMB sector

Fig. 3: Convergence of the proposed RCG algorithm with different number of STAR-RIS elements.

with the initial values selected for the algorithm. When the initial values of the optimization variables are close to the optimal solution, the algorithm requires fewer iterations to converge. Overall, the proposed RCG algorithm demonstrates strict convergence with a relatively low number of iterations needed.

3) Impact of the number of STAR-RIS elements:

In Fig. 4, we assess the impact of the number of STAR-RIS elements on the achievable rate, maintaining the transmit power at a constant 0 dBm. Note that as the number of STAR-RIS elements increases, the achievable rate of the CCU also increases. However, with the increase of STAR-RIS elements, the achievable rate of the CEU remains relatively constant. The phenomenon suggests that we can improve the SINR of the CCU by increasing the number of STAR-RIS elements, and thus improve the achievable rate of the CCU. However, the achievable rate of the CEU is determined primarily by the NOMA power allocation factors, which is independent of both the number of STAR-RIS elements and their reflection power coefficient. Furthermore, an analysis of the three solid lines in the figure reveals that the reflection and transmission power coefficient of STAR-RIS elements have a significant influence

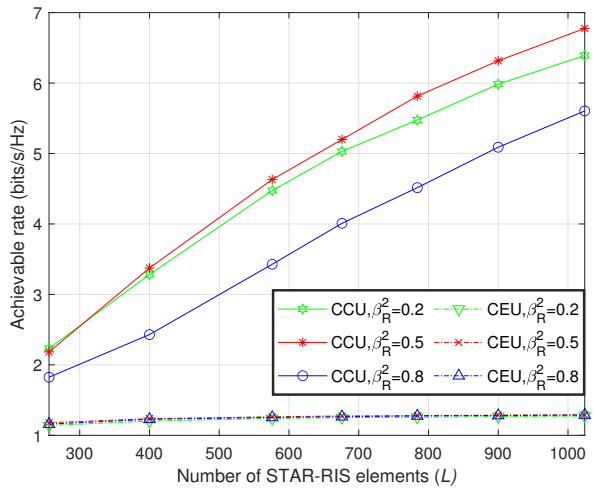

Fig. 4: Achievable rate versus the number of STAR-RIS elements.

on the proposed SSEIM design. Notably, when the reflection power coefficient of STAR-RIS is set at 0.8, the achievable rate for the CCU is substantially reduced.

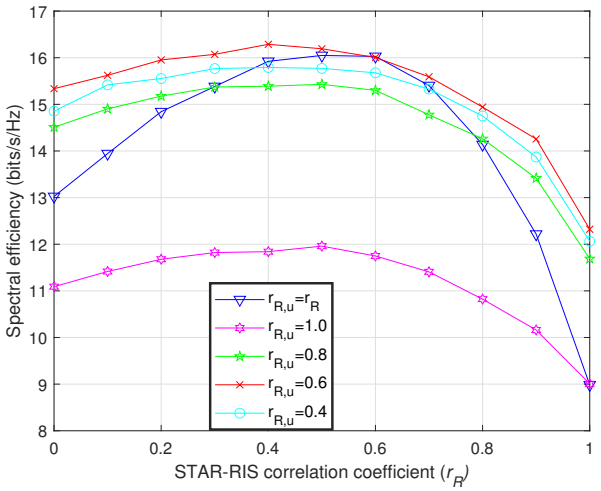

Fig. 5: SE versus the correlation coefficient when $\beta_R^2 = 0.5$.

4) Impact of the correlation coefficients:

Fig. 5 illustrates the spectral efficiency of STAR-RIS assisted cellular MISO-NOMA network versus the correlation coefficients $r_{R,u}$ and r_R. As the correlation coefficient of STAR-RIS r_R increases, SE initially shows an increase. It is because that a moderate increase in the STAR-RIS correlation coefficient r_R makes the phase adjustment more regular. Therefore, it is very necessary to miniaturize RIS array [22]. However, beyond a certain point, further increases in r_R lead to a decline in SE. It is due to the fact that the augmented spatial correlation lessens the spatial diversity [23]. Furthermore, Fig. 5 shows that as the correlation coefficient from STAR-RIS to users $r_{R,u}$ increases, the spectral efficiency continuously declines. Due to the restrictions on the possible phase shifts of STAR-RIS elements and the signal adjustment

of users, we observe an extremely poor spectral efficiency [24]. The analysis highlights the critical impact of correlation coefficients on the performance of spectral efficiency.

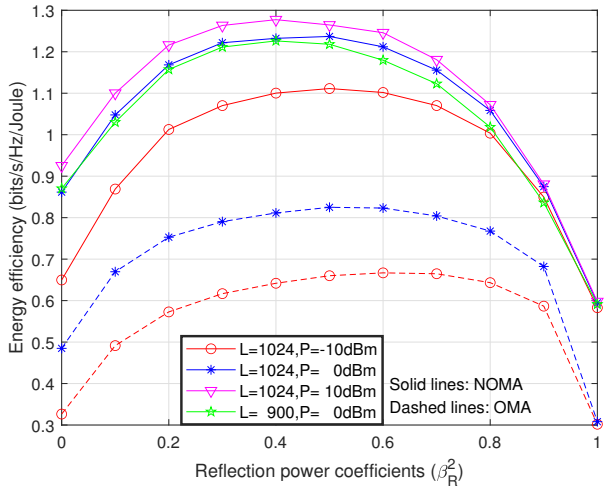

Fig. 6: EE versus the reflection power coefficients with different transmit power of BSs and different number of STAR-RIS elements, where the static power of users $P_U = 10$dBm, the static power of BS $P_{B,s} = 9$dBW, the amplifier efficiency at BS $\varepsilon_b = 1.2$.

5) Impact of the reflection coefficients:

We focus on the energy efficiency in relation to the reflection power coefficient, as illustrated in Fig. 6. As the reflection power coefficient increases, the system's energy efficiency initially rises rapidly, then stabilizes, and eventually declines sharply. Because the MRT precoding matrix optimizes the active beamforming at BSs, high energy efficiency is achieved when the reflection power coefficient of STAR-RIS elements is within an optimal range $\beta_R^2 \in [0.2, 0.7]$. In view of Fig. 2, it is clear that there is a trade-off between the SEB-sector and IMB-sector. The optimal reflection coefficient is not necessarily capable of completely mitigating interference. Additionally, the blue curve above the green curve demonstrates that the energy efficiency improves as the number of STAR-RIS elements increases. The pink curve at the highest position indicates that a higher transmit power leads to greater energy efficiency. Furthermore, it can be known by comparing the dashed curves and the solid curves in Fig. 6 that the system energy efficiency of the SSEIM design in the NOMA network is superior to that of the OMA network. Based on (59) and (60), we can adopt an appropriate number of STAR-RIS elements, employ technologies like deep sleeping and sub-frame silence to achieve energy conservation in wireless networks without affecting system performance [20].

6) Compare with different baseline schemes:

Fig. 7(a) investigates the spectral efficiency of the proposed SSEIM design in comparison with four benchmark schemes: RIS-aided SEB design, RIS-aided IMB design, no STAR-RIS and random STAR-RIS. The blue curve at the highest position indicates that the proposed STAR-RIS assisted SSEIM design achieves significantly higher spectral efficiency than other

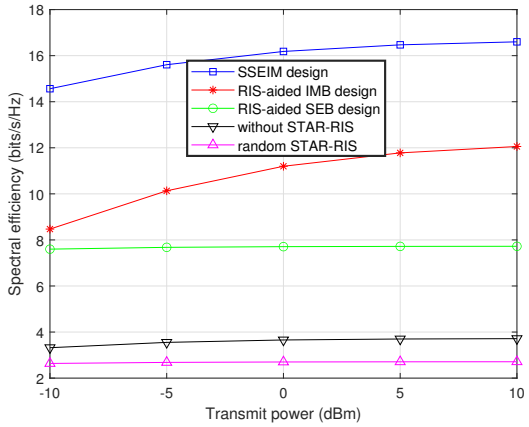

(a) SE versus the transmit power.

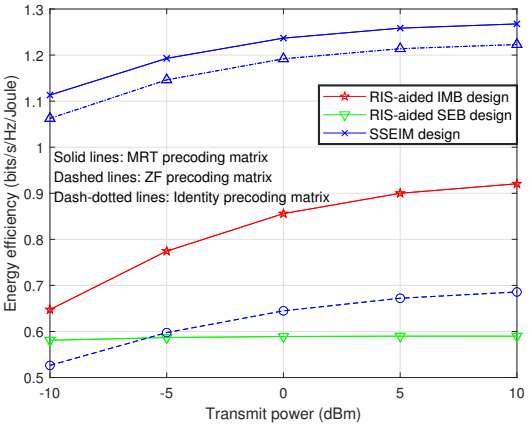

(b) EE versus the transmit power.

Fig. 7: Different baseline schemes in the case of the reflection power coefficient of STAR-RIS $\beta_R^2 = 0.5$, the number of STAR-RIS elements $L = 1024$.

baseline schemes, demonstrating its superior performance over traditional approaches. From Fig. 7(a), we can also draw the following conclusions: i) As the transmit power of BSs increases, the spectral efficiency of both the proposed SSEIM design and RIS-aided IMB design continually increases. However, the spectral efficiency of RIS-aided SEB design does not change significantly with increasing transmit power; ii) The STAR-RIS assisted design outperforms the design without STAR-RIS; iii) If the phase shifts of STAR-RIS elements are random, its performance is the worst; iv) In the STAR-RIS assisted cellular MISO-NOMA network using the MRT precoding matrix, the performance of RIS-aided IMB design is better than that of RIS-aided SEB design.

Utilizing the same parameters as above, Fig. 7(b) compares the energy efficiency of different baseline schemes and precoding strategies. Considering the MRT precoding matrix, ZF precoding matrix and identity precoding matrix, the solid blue line is significantly higher than the dashed and dotted lines. It indicates that the proposed MRT precoding matrix, which jointly optimizes the active beamforming at BSs and the passive beamforming of the STAR-RIS, achieves higher

energy efficiency than the ZF and identity precoding matrices. Additionally, the blue curve is much higher than the green and red curves, demonstrating that the proposed SSEIM design has a performance advantage, achieving higher energy efficiency than other baseline schemes. In summary, the SSEIM design based on the MRT precoding matrix exhibits the most superior energy efficiency performance.

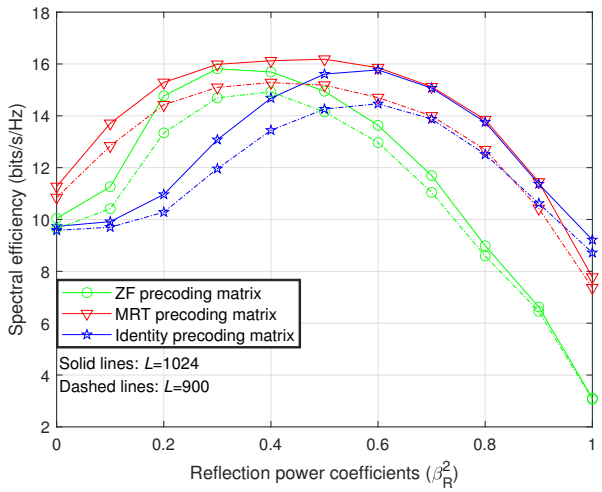

Fig. 8: SE versus the reflection power coefficients with different transmit power, different number of STAR-RIS elements as well as different precoding matrices.

7) Compare with different precoding matrices:

We plot the curves of system spectral efficiency versus the reflection power coefficient of STAR-RIS elements with different precoding matrices in Fig. 8. The solid lines consistently being above the dashed lines indicate that the spectral efficiency of the proposed SSEIM design improves as the number of STAR-RIS elements increases. No matter which precoding strategy is used, as the reflection power coefficient of STAR-RIS elements increases from 0 to 1, the system spectral efficiency first rises and then falls. When the reflection power coefficient reaches a specific value, the spectral efficiency attains its optimal level. By comparing the different colored curves, it can be seen that when using the MRT precoding matrix, the required reflection power coefficient to achieve optimal spectral efficiency falls within a range $\beta_R^2 \in [0.2, 0.8]$. Due to the active beamforming weights at BSs, the SE can maintain stability within this range. In contrast, when using the ZF precoding matrix and the identity precoding matrix, the required reflection power coefficient is a specific value. When the reflection power coefficient $\beta_R^2 \approx 0.3$ for the ZF precoding matrix or the reflection power coefficient $\beta_R^2 \approx 0.6$ for the identity precoding matrix, the desired signals are enhanced substantially and the interference signal is mitigated effectively, the SE reaches the peak value and the reflection coefficient reaches the optimal value. With further increasing of β_R, the SINR is dominated by the interference signals. At present, the interference can not be effectively mitigated.

Based on the above simulation results, two remarks are concluded.

Remark 1. *Compared to the RIS-aided SEB and IMB designs, the proposed SSEIM design has the best performance on both spectral efficiency and energy efficiency, which demonstrates the superiority of the proposed SSEIM design.*

Remark 2. *The proposed SSEIM-aided network with MRT precoding matrix outperforms the SSEIM-aided network with the identity precoding matrix and ZF precoding matrix. It indicates that the MRT precoding matrix can reduce the limitations on the reflection and transmission coefficients of STAR-RIS in practical engineering.*

VI. Conclusion

In this paper, we proposed a novel dual-sided STAR-RIS-assisted SSEIM design for the multiuser MISO-NOMA downlink cellular networks. Around the objective of maximizing the system spectral efficiency, we jointly optimized the transmission and reflection phase shifts at the STAR-RIS, the precoding matrix of BSs, and the power allocation factors of NOMA users. Specifically, we first maximized the effective channel power gain, and then minimized the interferences. Finally, we optimized the NOMA power allocation factors based on the target data rates. We proposed a LSEM algorithm, where both the non-convex unit modulus constraint subproblems were solved by the RCG algorithm. Numerical results illustrated that the STAR-RIS-assisted SSEIM design can significantly improve the SE and EE of the cellular MISO-NOMA networks. We also demonstrated that the MRT precoding matrix has the best performance compared to other precoding strategies. However, in practical scenarios, due to the constraints of factors like buildings and terrain, it is not easy to find a suitable deployment location. In addition, the protocols of existing communication systems need to be modified or optimized to make them compatible with STAR-RIS in order to achieve seamless integration and application. This is also the direction of our future research.

References

[1] Y. Liu, X. Liu, X. Mu, T. Hou, J. Xu, M. Di Renzo, and N. Al-Dhahir, "Reconfigurable intelligent surfaces: Principles and opportunities," *IEEE Commun. Surveys Tuts.*, vol. 23, no. 3, pp. 1546–1577, 3rd Quart. 2021.

[2] S. Zeng, H. Zhang, B. Di, Z. Han, and L. Song, "Reconfigurable intelligent surface (RIS) assisted wireless coverage extension: RIS orientation and location optimization," *IEEE Commun. Lett.*, vol. 25, no. 1, pp. 269–273, Jan. 2021.

[3] K. Asmoro and S. Y. Shin, "RIS grouping based index modulation for 6G telecommunications," *IEEE Wireless Commun. Lett.*, vol. 11, no. 11, pp. 2410–2414, Nov. 2022.

[4] M. Di Renzo, A. Zappone, M. Debbah, M.-S. Alouini, C. Yuen, J. de Rosny, and S. Tretyakov, "Smart radio environments empowered by reconfigurable intelligent surfaces: How it works, state of research, and the road ahead," *IEEE J. Sel. Areas Commun.*, vol. 38, no. 11, pp. 2450–2525, Nov. 2020.

[5] X. Mu, Y. Liu, L. Guo, J. Lin, and R. Schober, "Intelligent reflecting surface enhanced indoor robot path planning: A radio map-based approach," *IEEE Trans. Wireless Commun.*, vol. 20, no. 7, pp. 4732–4747, Jul. 2021.

[6] A. R. Ndjiongue, T. M. N. Ngatched, O. A. Dobre, and H. Haas, "Toward the use of re-configurable intelligent surfaces in VLC systems: Beam steering," *IEEE Wireless Commun.*, vol. 28, no. 3, pp. 156–162, Jun. 2021.

[7] X. Mu, J. Xu, Y. Liu, and L. Hanzo, "Reconfigurable intelligent surface-aided near-field communications for 6G: Opportunities and challenges," *IEEE Veh. Technol. Mag.*, vol. 19, no. 1, pp. 65–74, Mar. 2024.

[8] Y. Liu, X. Mu, J. Xu, R. Schober, Y. Hao, H. V. Poor, and L. Hanzo, "STAR: simultaneous transmission and reflection for 360° coverage by intelligent surfaces," *IEEE Wireless Commun.*, vol. 28, no. 6, pp. 102–109, Dec. 2021.

[9] J. Xu, Y. Liu, X. Mu, and O. A. Dobre, "STAR-RISs: Simultaneous transmitting and reflecting reconfigurable intelligent surfaces," *IEEE Commun. Lett.*, vol. 25, no. 9, pp. 3134–3138, Sep. 2021.

[10] X. Mu, Y. Liu, L. Guo, J. Lin, and R. Schober, "Simultaneously transmitting and reflecting (STAR) RIS aided wireless communications," *IEEE Trans. Wireless Commun.*, vol. 21, no. 5, pp. 3083–3098, May 2022.

[11] J. Xu, X. Mu, J. T. Zhou, and Y. Liu, "Simultaneously transmitting and reflecting (STAR)-RISs: Are they applicable to dual-sided incidence?" *IEEE Wireless Commun. Lett.*, vol. 12, no. 1, pp. 129–133, Nov. 2023.

[12] Z. Wang, X. Mu, and Y. Liu, "STARS enabled integrated sensing and communications," *IEEE Trans. Wireless Commun.*, vol. 22, no. 10, pp. 6750–6765, Oct. 2023.

[13] Z. Wang, X. Mu, J. Xu, and Y. Liu, "Simultaneously transmitting and reflecting surface (STARS) for terahertz communications," *IEEE J. Sel. Areas Commun.*, vol. 17, no. 4, pp. 861–877, Jul. 2023.

[14] Y. Pan, Z. Qin, J.-B. Wang, Y. Chen, H. Yu, and A. Tang, "Joint deployment and beamforming design for STAR-RIS aided communication," *IEEE Commun. Lett.*, vol. 27, no. 11, pp. 3083–3087, Nov. 2023.

[15] M. A. ElMossallamy, K. G. Seddik, W. Chen, L. Wang, G. Y. Li, and Z. Han, "RIS optimization on the complex circle manifold for interference mitigation in interference channels," *IEEE Trans. Veh. Technol.*, vol. 70, no. 6, pp. 6184–6189, Jun. 2021.

[16] J. Li, Z. Song, T. Hou, X. Sun, A. Li, and E. Bodanese, "An RIS-NOMA-enhanced signal-cancellation design for multi-cell networks," in *Proc. IEEE Globecom Workshops (GC Wkshps)*, Dec. 2022, pp. 1022–1027.

[17] T. Hou, Y. Liu, Z. Song, X. Sun, Y. Chen, and L. Hanzo, "MIMO assisted networks relying on intelligent reflective surfaces: A stochastic geometry based analysis," *IEEE Trans. Veh. Technol.*, vol. 71, no. 1, pp. 571–582, Jan. 2022.

[18] M. Li, S. Zhang, Y. Ge, Z. Li, F. Gao, and P. Fan, "STAR-RIS aided integrated sensing and communication over high mobility scenario," *IEEE Trans. Commun.*, vol. 72, no. 8, pp. 4788–4802, Aug. 2024.

[19] W. Ni, Y. Liu, Y. C. Eldar, Z. Yang, and H. Tian, "STAR-RIS integrated nonorthogonal multiple access and over-the-air federated learning: Framework, analysis, and optimization," *IEEE Internet Things J.*, vol. 9, no. 18, pp. 17 136–17 156, Sep. 2022.

[20] J. Li, Z. Song, T. Hou, J. Gao, A. Li, and Z. Tang, "An RIS-aided interference mitigation-based design for MIMO-NOMA in cellular networks," *IEEE Trans. Green Commun. Netw.*, vol. 8, no. 1, pp. 317–329, Mar. 2024.

[21] T. Hou, J. Wang, Y. Liu, X. Sun, A. Li, and B. Ai, "A joint design for STAR-RIS enhanced NOMA-CoMP networks: A simultaneous-signal-enhancement-and-cancellation-based (SSECB) design," *IEEE Trans. Veh. Technol.*, vol. 71, no. 1, pp. 1043–1048, Jan. 2022.

[22] Z. Abdullah, A. Papazafeiropoulos, S. Kisseleff, S. Chatzinotas, and B. Ottersten, "Impact of phase-noise and spatial correlation on double-RIS-assisted multiuser MISO networks," *IEEE Wireless Commun. Lett.*, vol. 11, no. 7, pp. 1473–1477, Jul. 2022.

[23] D. Yang, J. Xu, W. Xu, Y. Huang, and Z. Lu, "Secure communication for spatially correlated RIS-aided multiuser massive MIMO systems: Analysis and optimization," *IEEE Commun. Lett.*, vol. 27, no. 3, pp. 797–801, Mar. 2023.

[24] M.-M. Zhao, Q. Wu, M.-J. Zhao, and R. Zhang, "Intelligent reflecting surface enhanced wireless networks: Two-timescale beamforming optimization," *IEEE Trans. Wireless Commun.*, vol. 20, no. 1, pp. 2–17, Jan. 2021.

[25] C. Luo, W. Jiang, J. Nie, D. Niyato, C. Pan, Z. Xiong, and P. Xiong, "Robust beamforming design for the STAR-RIS-assisted secure SWIPT system," *IEEE Trans. Veh. Technol.*, pp. 1–14, 2024.

[26] B. Wang, X. Tao, S. Han, K. Yang, and H. Wu, "Secure transmission design for rate-splitting empowered STAR-RIS-Aided networks," *IEEE Wireless Commun. Lett.*, vol. 13, no. 9, pp. 2581–2585, Sep. 2024.

[27] X. Li, J. Li, Y. Liu, Z. Ding, and A. Nallanathan, "Residual transceiver hardware impairments on cooperative NOMA networks," *IEEE Trans. Wireless Commun.*, vol. 19, no. 1, pp. 680–695, Jan. 2020.

[28] A. S. d. Sena, D. Carrillo, F. Fang, P. H. J. Nardelli, D. B. d. Costa, U. S. Dias, Z. Ding, C. B. Papadias, and W. Saad, "What role do intelligent reflecting surfaces play in multi-antenna non-orthogonal multiple access?" *IEEE Wireless Commun.*, vol. 27, no. 5, pp. 24–31, Otc. 2020.

[29] Z. Zhang, C. Zhang, C. Jiang, F. Jia, J. Ge, and F. Gong, "Improving physical layer security for reconfigurable intelligent surface aided NOMA 6G networks," *IEEE Trans. Veh. Technol.*, vol. 70, no. 5, pp. 4451–4463, May 2021.

[30] B. Lyu, P. Ramezani, D. T. Hoang, and A. Jamalipour, "IRS-assisted downlink and uplink NOMA in wireless powered communication networks," *IEEE Trans. Veh. Technol.*, vol. 71, no. 1, pp. 1083–1088, Jan. 2022.

[31] H. Liu, G. Li, X. Li, Y. Liu, G. Huang, and Z. Ding, "Effective capacity analysis of STAR-RIS-assisted NOMA networks," *IEEE Wireless Commun. Lett.*, vol. 11, no. 9, pp. 1930–1934, Sep. 2022.

[32] J. Chen and X. Yu, "Ergodic rate analysis and phase design of STAR-RIS aided NOMA with statistical CSI," *IEEE Commun. Lett.*, vol. 26, no. 12, pp. 2889–2893, Dec. 2022.

[33] H. Ma, H. Wang, H. Li, and Y. Feng, "Transmit power minimization for STAR-RIS-empowered uplink NOMA system," *IEEE Wireless Commun. Lett.*, vol. 11, no. 11, pp. 2430–2434, Nov. 2022.

[34] C. Wu, Y. Liu, X. Mu, X. Gu, and O. A. Dobre, "Coverage characterization of STAR-RIS networks: NOMA and OMA," *IEEE Commun. Lett.*, vol. 25, no. 9, pp. 3036–3040, Sep. 2021.

[35] J. Zuo, Y. Liu, Z. Ding, L. Song, and H. V. Poor, "Joint design for simultaneously transmitting and reflecting (STAR) RIS assisted NOMA systems," *IEEE Trans. Wireless Commun.*, vol. 22, no. 1, pp. 611–626, Jan. 2023.

[36] K. Zhi, C. Pan, H. Ren, and K. Wang, "Power scaling law analysis and phase shift optimization of RIS-aided massive MIMO systems with statistical CSI," *IEEE Trans. Commun.*, vol. 70, no. 5, pp. 3558–3574, May 2022.

[37] T. Hou, Y. Liu, Z. Song, X. Sun, and Y. Chen, "Multiple antenna aided NOMA in UAV networks: A stochastic geometry approach," *IEEE Trans. Commun.*, vol. 67, no. 2, pp. 1031–1044, Feb. 2019.

[38] C. Zhou, B. Lyu, C. You, and Z. Liu, "Movable antenna enabled symbiotic radio systems: An opportunity for mutualism," *IEEE Wireless Commun. Lett.*, pp. 1–1, 2024.

[39] S. Mishra, L. Salaun, H. Yang, and C. S. Chen, "Graph neural network aided power control in partially connected cell-free massive MIMO," *IEEE Trans. Wireless Commun.*, vol. 23, no. 9, pp. 12 412–12 423, Sep. 2024.

[40] Y. Chen, M. Wen, E. Basar, Y.-C. Wu, L. Wang, and W. Liu, "Exploiting reconfigurable intelligent surfaces in edge caching: Joint hybrid beamforming and content placement optimization," *IEEE Trans. Wireless Commun.*, vol. 20, no. 12, pp. 7799–7812, Dec. 2021.

[41] X. Yu, D. Xu, and R. Schober, "MISO wireless communication systems via intelligent reflecting surfaces," in *Proc. IEEE/CIC Int. Conf. Commun. China (ICCC), Changchun, China*, Aug. 2019, pp. 735–740.

[42] C. Pan, H. Ren, K. Wang, W. Xu, M. Elkashlan, A. Nallanathan, and L. Hanzo, "Multicell MIMO communications relying on intelligent reflecting surfaces," *IEEE Trans. Wireless Commun.*, vol. 19, no. 8, pp. 5218–5233, Aug. 2020.

[43] L. N. Ribeiro, S. Schwarz, M. Rupp, and A. L. F. de Almeida, "Energy efficiency of mmWave massive MIMO precoding with low-resolution DACs," *IEEE J. Sel. Topics. Signal Process*, vol. 12, no. 2, pp. 298–312, May 2018.

[44] Z. Zhai, X. Dai, B. Duo, X. Wang, and X. Yuan, "Energy-efficient UAV-mounted RIS assisted mobile edge computing," *IEEE Wireless Commun. Lett.*, vol. 11, no. 12, pp. 2507–2511, Dec. 2022.

[45] P.-A. Absil, R. Mahony, and R. Sepulchre, *Optimization Algorithms on Matrix Manifolds*. Princeton University Press, 2008.

[46] K. Zhi, C. Pan, G. Zhou, H. Ren, M. Elkashlan, and R. Schober, "Is RIS-aided massive MIMO promising with ZF detectors and imperfect CSI?" *IEEE J. Sel. Areas Commun.*, vol. 40, no. 10, pp. 3010–3026, Oct. 2022.

[47] T. Hou, Y. Liu, Z. Song, X. Sun, and Y. Chen, "MIMO-NOMA networks relying on reconfigurable intelligent surface: A signal cancellation-based design," *IEEE Trans. Commun.*, vol. 68, no. 11, pp. 6932–6944, Nov. 2020.

[48] A. M. Auyo, S. A. Babale, and L. M. Bello, "Effect of inspired CR-NOMA power allocation on bit error rate for three user NOMA system," in *Proc. IEEE Nigeria 4th Int. Conf. Disruptive Technol. for Sustain. Develop. (NIGERCON)*, Apr. 2022, pp. 1–5.

[49] Y. Wang, M. Tao, and S. Sun, "Cramér-Rao bound analysis and beamforming design for integrated sensing and communication with extended targets," *IEEE Trans. Wireless Commun.*, pp. 1–1, 2024.

[50] M. Li, W. Liu, J. Lei, J. Zhu, K. An, and S. Chatzinotas, "Integrated OTFS waveform design based on unified matrix for joint communication and radar system," *IEEE Internet Things J.*, vol. 11, no. 18, pp. 29 235–29 251, Sep. 2024.

Jie Li received the M.Sc. degree from the School of Electronic and Information Engineering, Beijing Jiaotong University, Beijing, China, in 2024. She is currently working with the China Mobile Research and Development Center for Network Planning and Optimization, China Mobile Group Design Institute Company Ltd., Beijing, China. Her research interests are in the field of B5G and 6G wireless communications, including but not limited to reconfigurable intelligent surfaces, next-generation multiple access, energy-saving and carbon reduction technologies.

Zhengyu Song (Member, IEEE) received the B.Sc. and M.Sc. degrees in information and communication engineering from Beijing Jiaotong University, Beijing, China, in 2008 and 2011, respectively, and the Ph.D. degree in information and communication engineering from Beijing Institute of Technology, Beijing, in 2016.,He is currently with the School of Electronic and Information Engineering, Beijing Jiaotong University. His main research interests include nonorthogonal multiple access, mobile-edge computing, reconfigurable intelligent surfaces, unmanned aerial vehicle, and terrestrial-satellite-integrated communications.

Tianwei Hou (S'19—M'21) received Ph.D. degree from Beijing Jiaotong University (BJTU) in 2021. He was a visiting scholar at Queen Mary University of London (QMUL) (Sep. 2018- Nov. 2020). Since 2021, he has been an associate professor at BJTU. Dr. Hou's current research interests include next generation multiple access (NGMA), reconfigurable intelligent surface (RIS) aided communications, UAV communications, multiuser multiple-input multiple-output (MIMO) communications, and stochastic geometry. He has granted a Marie Sklodowska-Curie fellowship by European Research Executive Agency in 2023. He has been selected as a young elite scientist sponsorship program by China Association for Science and Technology in 2022. He received the Exemplary Reviewer of the IEEE COMMUNICATION LETTERS and the IEEE TRANSACTIONS ON COMMUNICATIONS in 2018, 2019 and 2022. He has served as a TPC Member for many IEEE conferences, such as GLOBECOM, VTC, etc. He served as the publicity officer for the Next Generation Multiple Access Emerging Technology Initiative (NGMA-ETI). He has served as a Co-Chair in the 2nd, 4th and 5th NGMA-for-future-wireless-communication workshops in IEEE VTC 2022-Fall, IEEE VTC 2023-spring, IEEE ISCT-2022 and IEEE PIMRC 2023. He has also served as a co-chair in the RIS and Smart Environments Symposium of IEEE ICCT 2023. He serves as the leading Guest Editor for IEEE IoT-J special issue on Next Generation Multiple Access for Internet of Things.

Chongwen Huang obtained his B. Sc. degree in 2010 from Nankai University, and the M.Sc degree from the University of Electronic Science and Technology of China in 2013, and PhD degree from Singapore University of Technology and Design (SUTD) in 2019. From Oct. 2019 to Sep. 2020, he is a Postdoc in SUTD. Since Sep. 2020, he joined into Zhejiang University as a tenure-track young professor. Dr. Huang is the recipient of 2021 IEEE Marconi Prize Paper Award, 2023 IEEE Fred W. Ellersick Prize Paper Award and 2021 IEEE ComSoc Asia-Pacific Outstanding Young Researcher Award. He has served as an Editor of IEEE Communications Letter, Elsevier Signal Processing, EURASIP Journal on Wireless Communications and Networking and Physical Communication since 2021. His main research interests are focused on Holographic MIMO Surface/Reconfigurable Intelligent Surface, B5G/6G Wireless Communications, mmWave/THz Communications, Deep Learning technologies for Wireless communications, etc.

Anna Li received her Ph.D. degree in Computer Science from the School of Electronic Engineering and Computer Science, Queen Mary University of London, London, U.K., in 2023. She has been a Lecturer in the School of Computing and Communications at Lancaster University, Lancaster, U.K., since September 2023. She is also a Marie Curie Fellow at Katholieke Universiteit Leuven (KU Leuven), Leuven, Belgium. Her research expertise encompasses wireless sensing, satellite navigation and communication systems, signal processing, and deep learning.

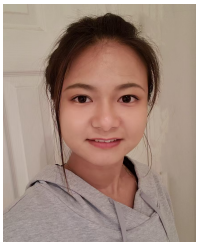

Gui Zhou (Member, IEEE) received the B.S. and M.E. degrees in Information and Electronics from Beijing Institute of Technology, Beijing, China, in 2015 and 2019, respectively, and the Ph.D. degree in Electronic Engineering and Computer Science from Queen Mary University of London, U.K. in 2022. She was a Humboldt Post-Doctoral Research Fellow at the Institute for Digital Communications from Friedrich-Alexander Universität of Erlangen-Nüremberg (FAU), Erlangen, Germany, from 2022-2024, where she is currently a Post-Doctoral Research Fellow. Her major research interests include channel estimation, transceiver design, integrated sensing and communication, and array signal processing. She is currently an Editor of IEEE Transactions on Communications.

Yuanwei Liu (Fellow, IEEE) received the Ph.D. degree from the Queen Mary University of London (QMUL), London, U.K., in 2016.

He is a tenured Full Professor with the Department of Electrical and Electronic Engineering (EEE), The University of Hong Kong (HKU); and a Visiting Professor with QMUL. Prior to that, he was a Senior Lecturer (an Associate Professor) (2021–2024) and a Lecturer (an Assistant Professor) (2017–2021) with QMUL; and a Post-Doctoral Research Fellow (2016–2017) with King's College London (KCL), London. His research interests include non-orthogonal multiple access, reconfigurable intelligent surface, near field communications, integrated sensing and communications, and machine learning. He is a fellow of AAIA; a Web of Science Highly Cited Researcher; an IEEE Communication Society Distinguished Lecturer; an IEEE Vehicular Technology Society Distinguished Lecturer; the Rapporteur of ETSI Industry Specification Group on Reconfigurable Intelligent Surfaces on work item of "Multi-Functional Reconfigurable Intelligent Surfaces (RIS): Modelling, Optimisation, and Operation;" and the U.K. Representative for the URSI Commission C on "Radio Communication Systems and Signal Processing." He was listed as one of 35 Innovators Under 35 China in 2022 by MIT Technology Review. He received the IEEE ComSoc Outstanding Young Researcher Award for EMEA in 2020, the 2020 IEEE Signal Processing and Computing for Communications (SPCC) Technical Committee Early Achievement Award, the IEEE Communication Theory Technical Committee (CTTC) 2021 Early Achievement Award, and the IEEE ComSoc Outstanding Nominee for Best Young Professionals Award in 2021. He was a co-recipient of the 2024 IEEE Communications Society Heinrich Hertz Award, the Best Student Paper Award in IEEE VTC2022-Fall, the Best Paper Award in ISWCS 2022, the 2022 IEEE SPCC-TC Best Paper Award, the 2023 IEEE ICCT Best Paper Award, and the 2023 IEEE ISAP Best Emerging Technologies Paper Award. He serves as the Publicity Co-Chair for IEEE VTC 2019-Fall; the Panel Co-Chair for IEEE WCNC 2024; and the Symposium Co-Chair for several flagship conferences, such as IEEE GLOBECOM, ICC, and VTC. He serves as the Academic Chair for the Next Generation Multiple Access Emerging Technology Initiative and the Vice Chair for SPCC and Technical Committee on Cognitive Networks (TCCN). He serves as the Co-Editor-in-Chief for IEEE ComSoc TC Newsletter; an Area Editor for IEEE TRANSACTIONS ON COMMUNICATIONS and IEEE COMMUNICATIONS LETTERS;an Editor for IEEE COMMUNICATIONS SURVEYS AND TUTORIALS,IEEE TRANSACTIONS ON WIRELESS COMMUNICATIONS,IEEE TRANSACTIONS ON VEHICULAR TECHNOLOGY,IEEE TRANSACTIONS ON NETWORK SCIENCE AND ENGINEERING,and IEEE TRANSACTIONS ON COGNITIVE COMMUNICATIONS AND NETWORKING. He serves as the (leading) Guest Editor for PROCEEDINGS OF THE IEEE on Next Generation Multiple Access, IEEE JOURNAL ON SELECTED AREAS IN COMMUNICATIONS on Next Generation Multiple Access, IEEE JOURNAL OF SELECTED TOPICS IN SIGNAL PROCESSING on Intelligent Signal Processing and Learning for Next Generation Multiple Access, and IEEE NETWORK on Next Generation Multiple Access for 6G. For more datails, please see https://www.eee.hku.hk/yuanwei/.